# $^{12}$Be structure study via resonant elastic scattering with ACTAR TPC

**Lou Dienis**

GANIL — Supervisors: F. de Oliveira Santos, N. de Séréville, C. Fougères

Colloque GANIL · September 22nd, 2026

# Clustering near decay thresholds

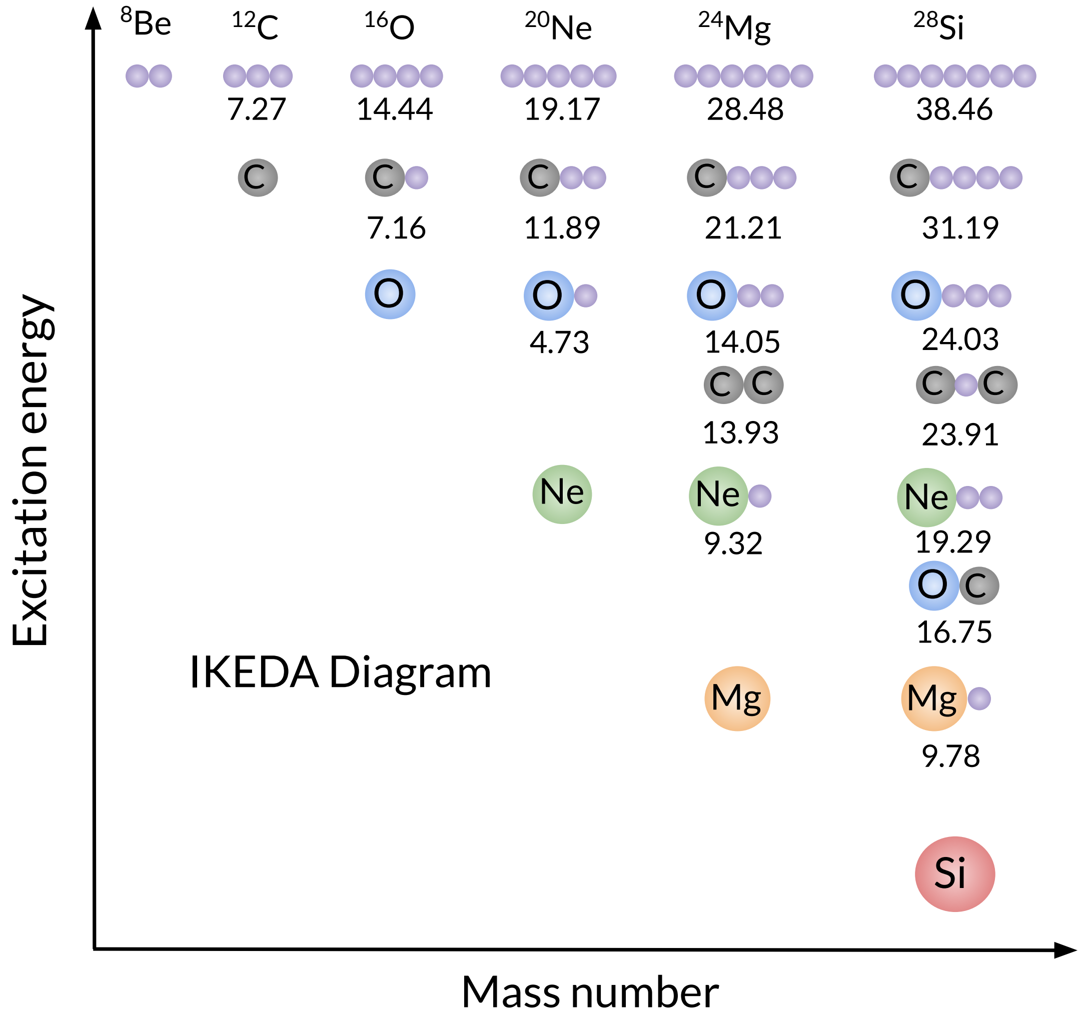


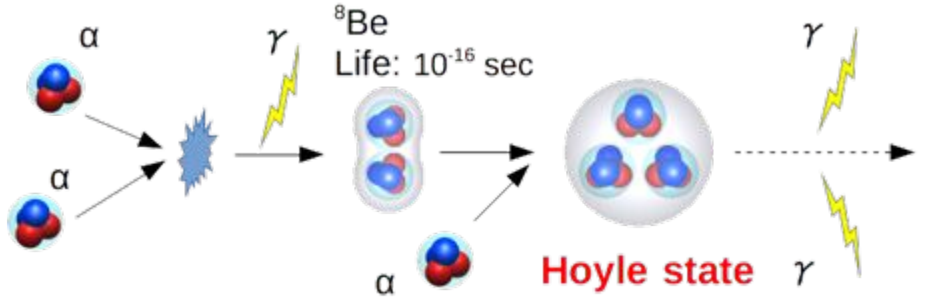


Department of Physics Tohoku University website

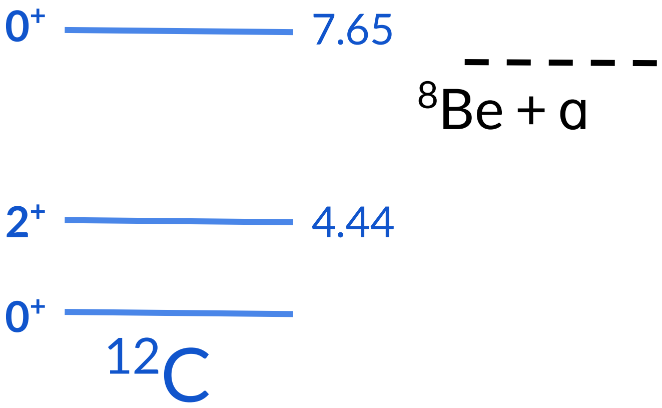


London Daily Express

# Clustering in Be

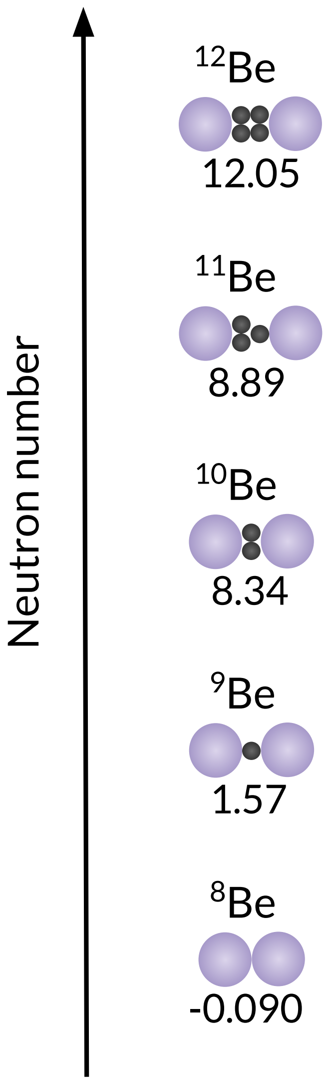


extended IKEDA diagram for $^{12}Be$ : molecular structure


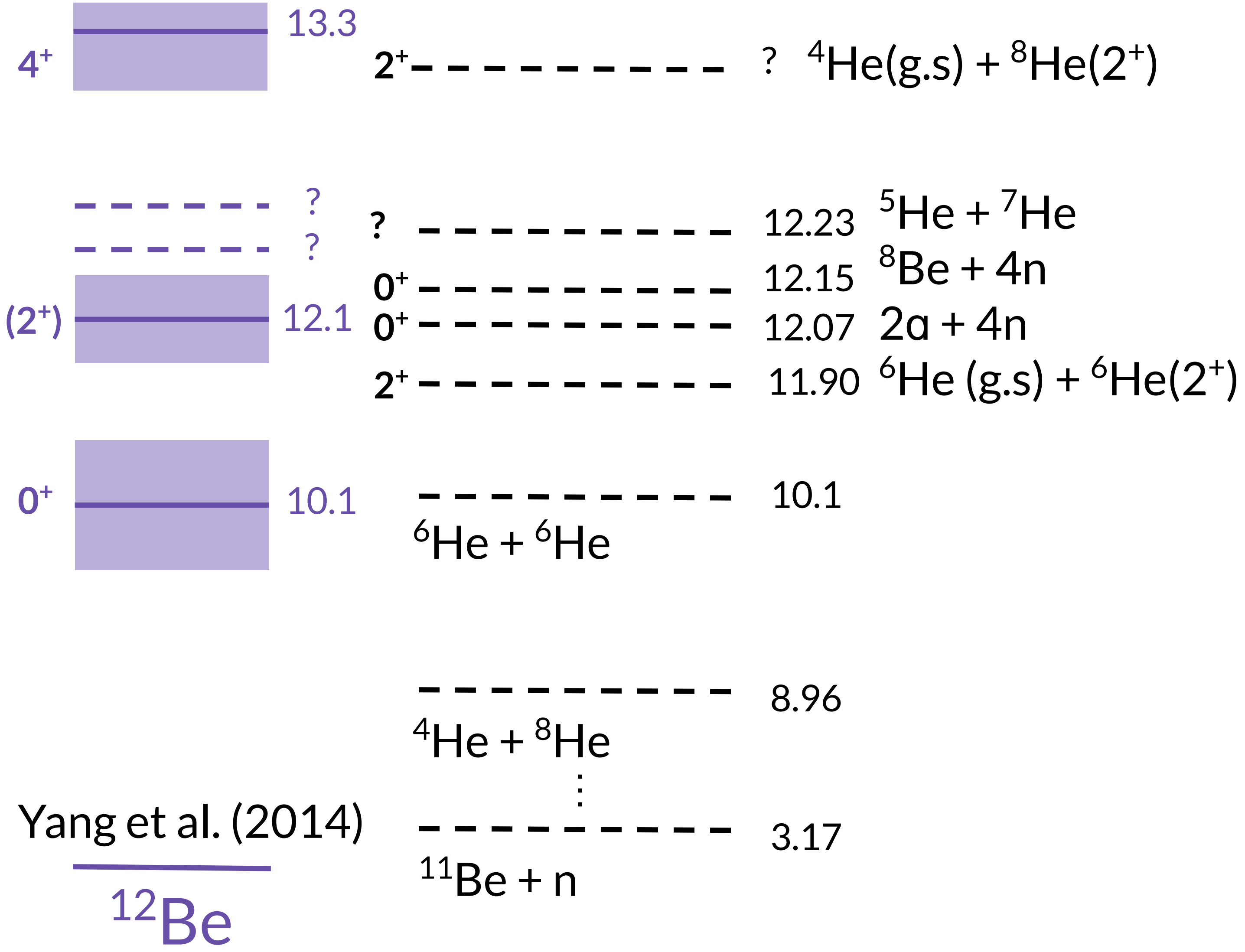

# ACTAR TPC

- Resonant elastic scattering reaction $^4He(^8He, ^8He)^4He$ -> population of $^{12}Be$ states
- $^8He$ beam at 1.8 MeV/u , and ACTAR TPC filled with $^4He$ gas

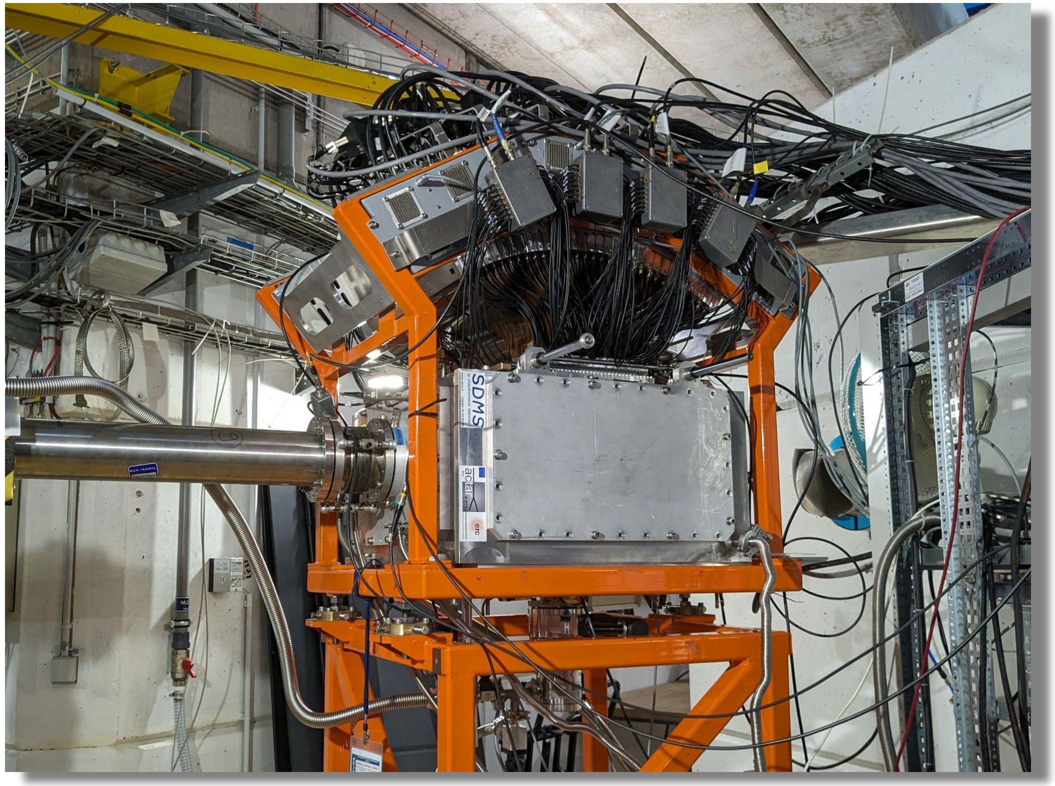


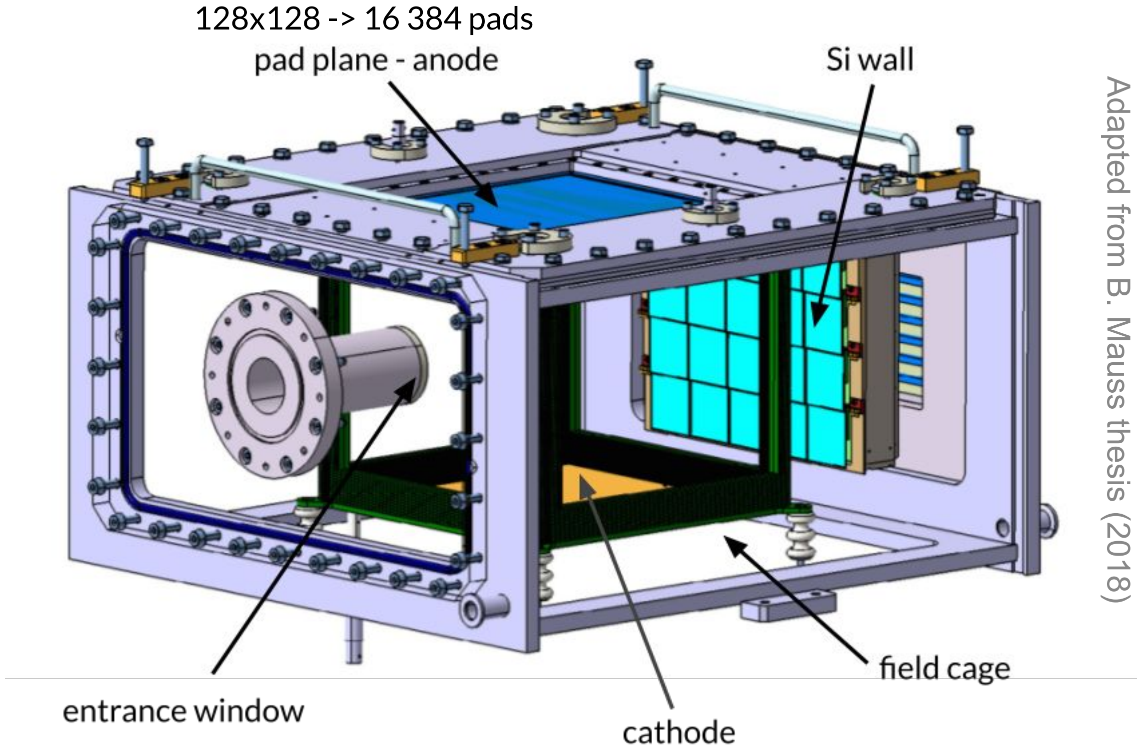


Adapted from B. Mauss thesis (2018)

# ACTAR TPC

- Resonant elastic scattering reaction $^4$He($^8$He, $^8$He)$^4$He -> population of $^{12}$Be states
- $^8$He beam at 1.8 MeV/u , and ACTAR TPC filled with $^4$He gas

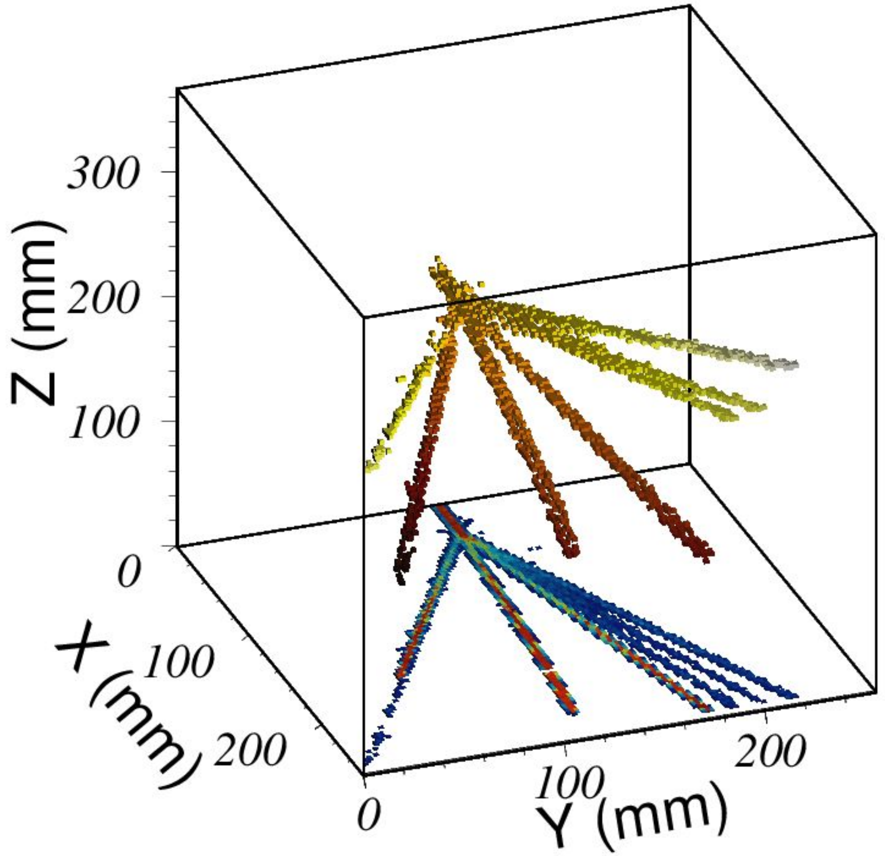


Source: GANIL website

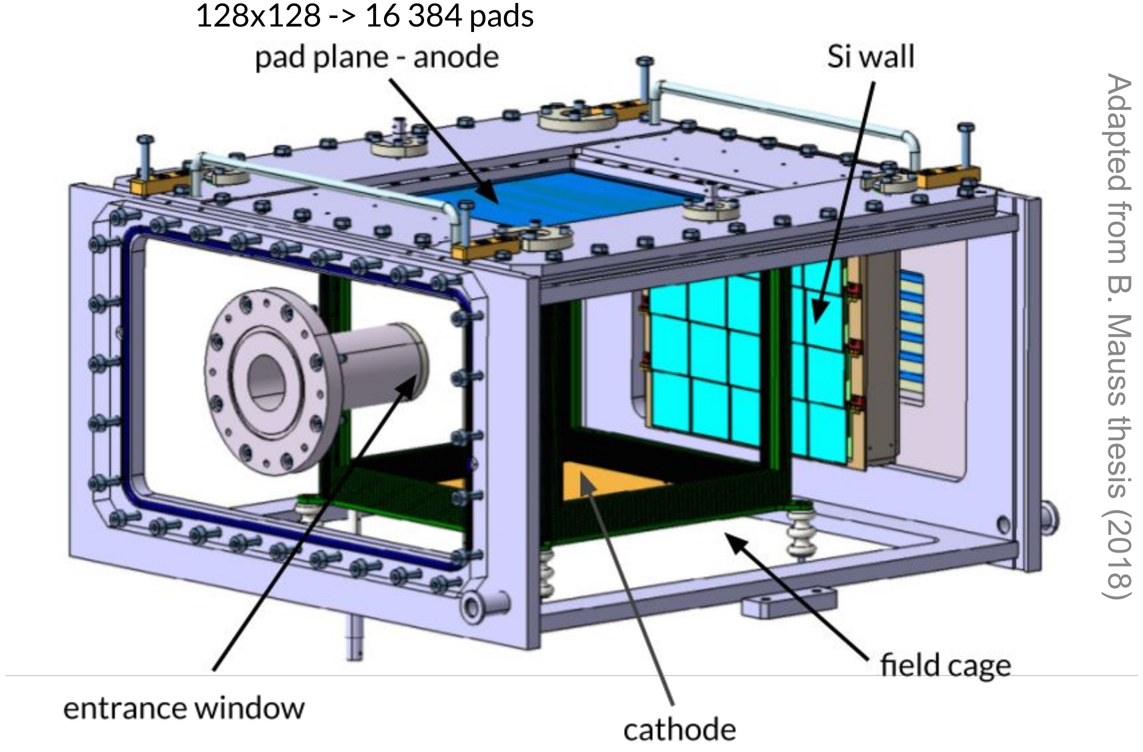


Adapted from B. Mauss thesis (2018)

# Resonant elastic scattering: $^{4}He(^{8}He,^{8}He)^{4}He$

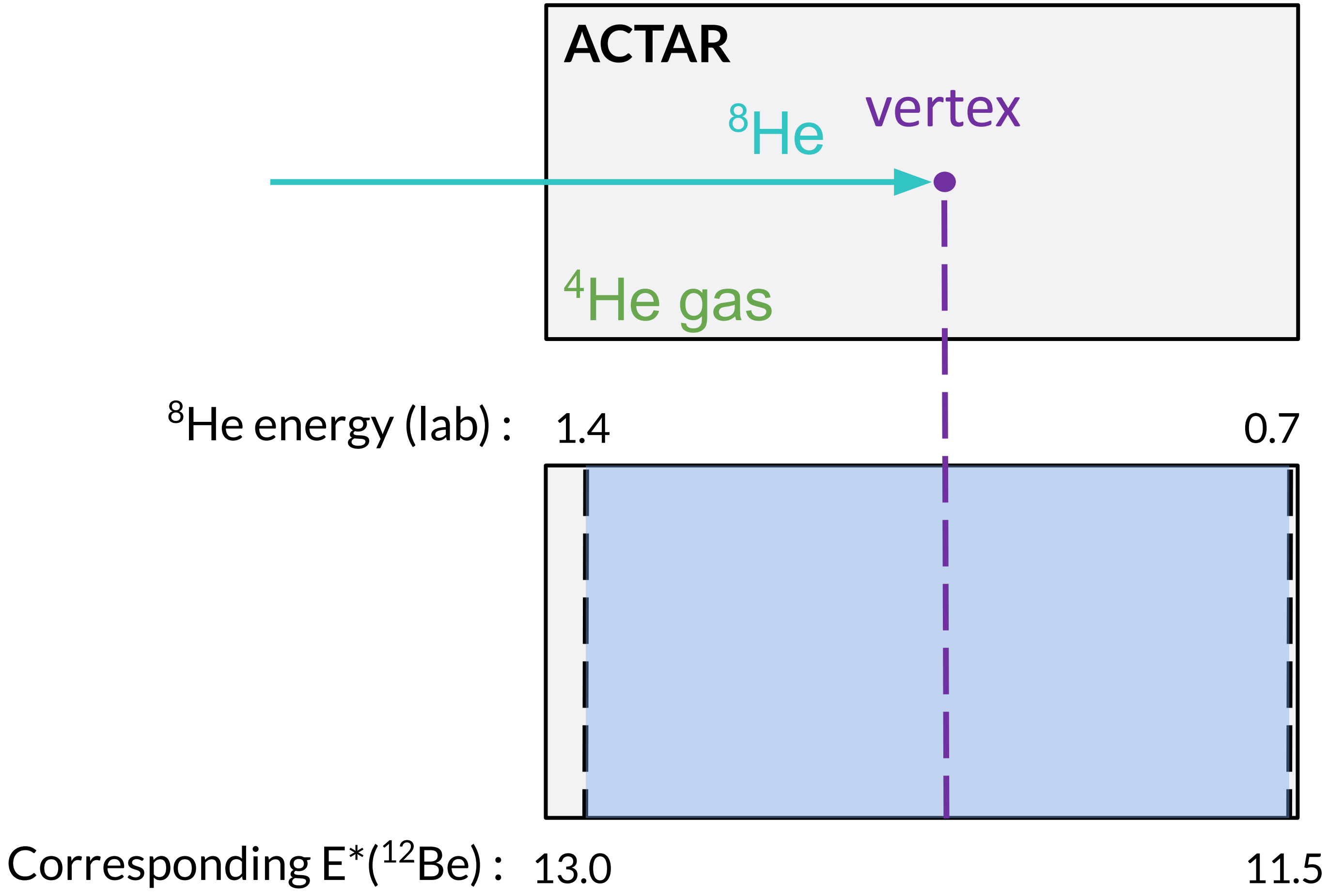


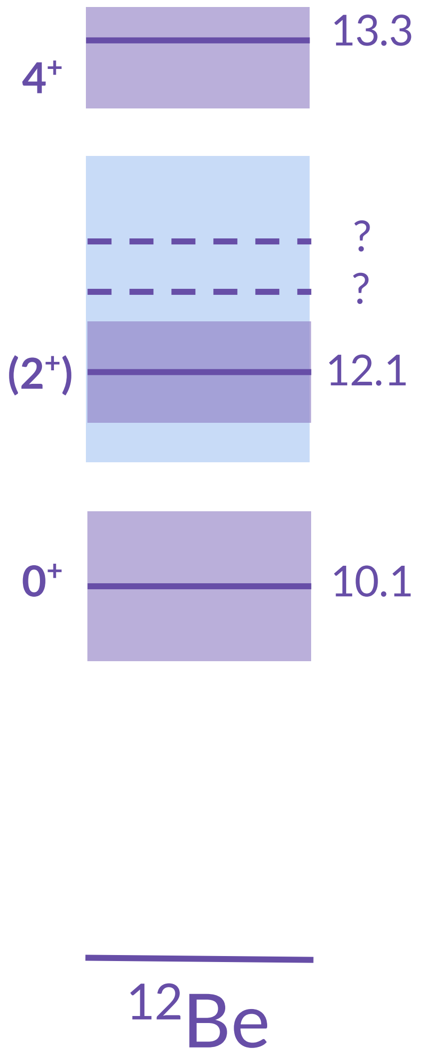

# Resonant elastic scattering: $^{4}He(^{8}He,^{8}He)^{4}He$

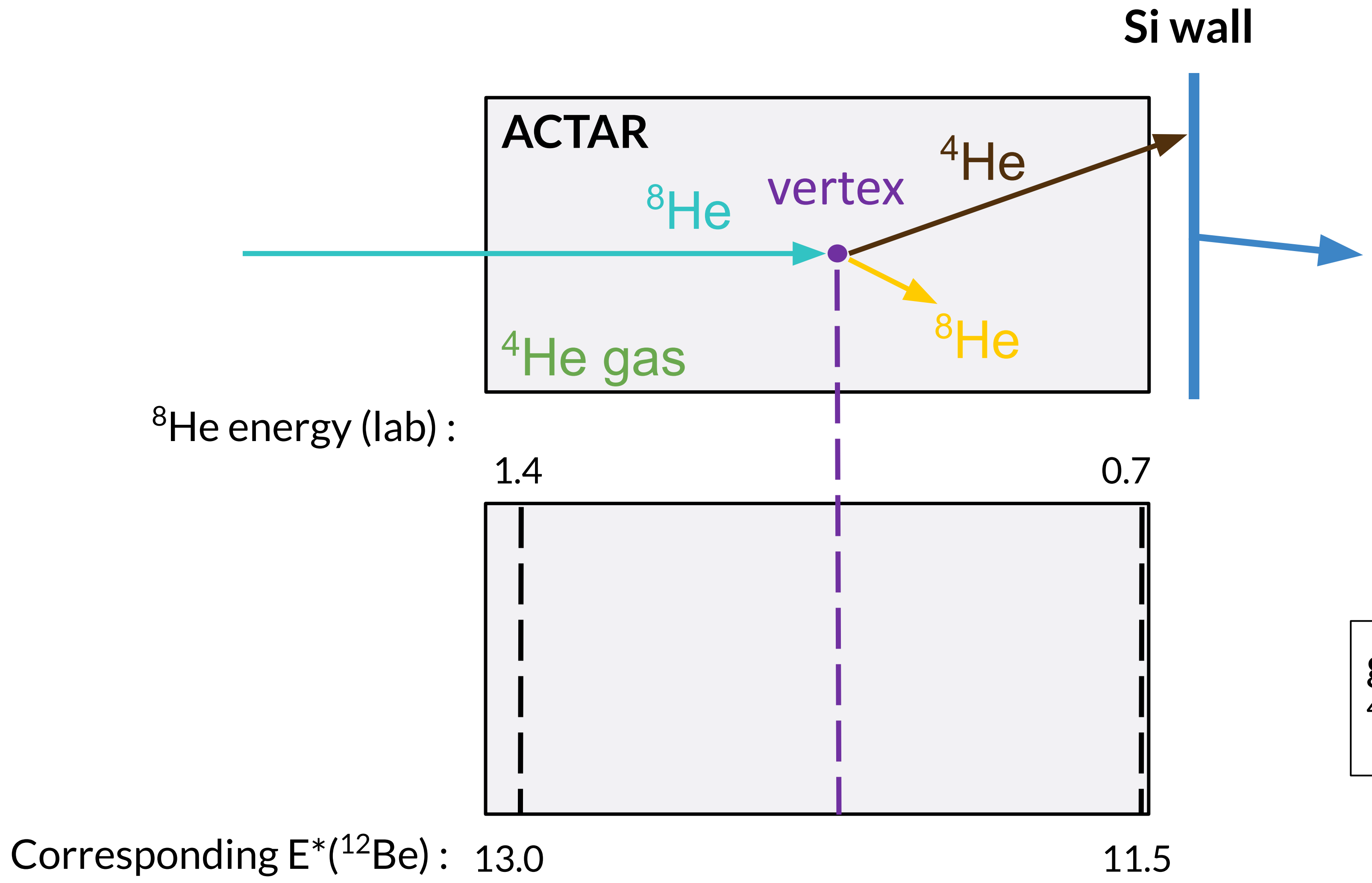


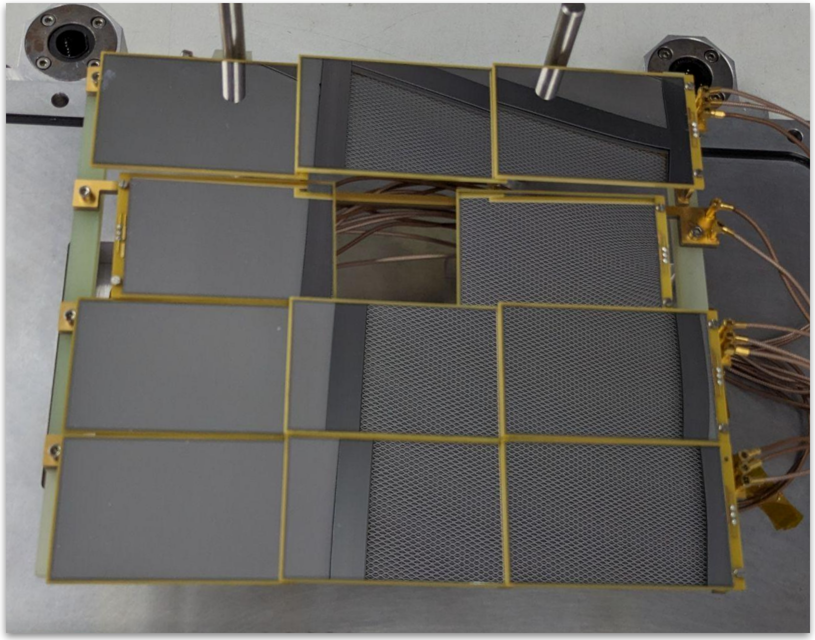

gas :
$^{4}He$ (97%) + $iC_4H_{10}$ (3%) @ 700 mbar

# Particle identification

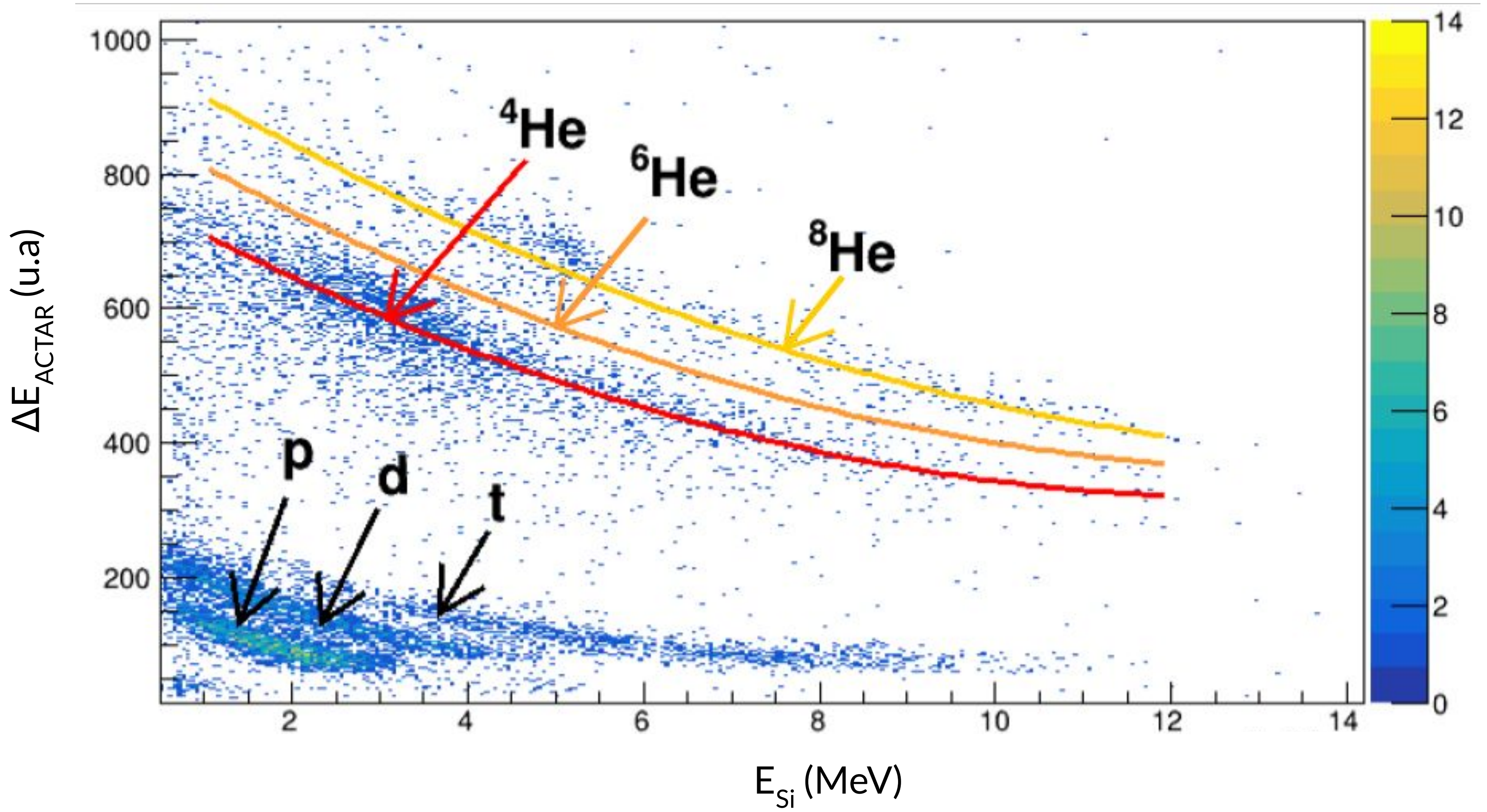

# Excitation energy

$\theta_{CM} \in [130°,140°]$

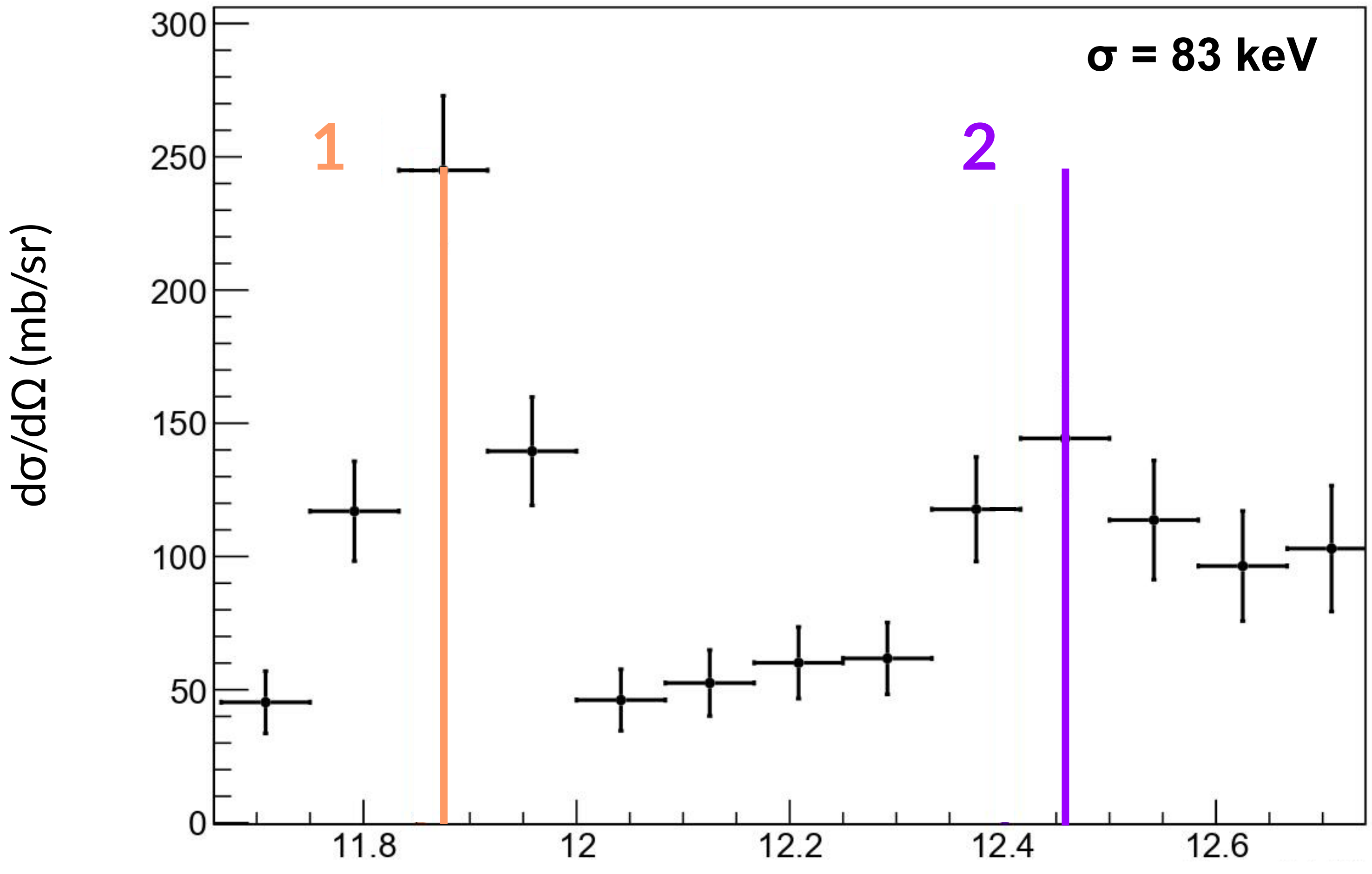


$E_x$ (MeV)

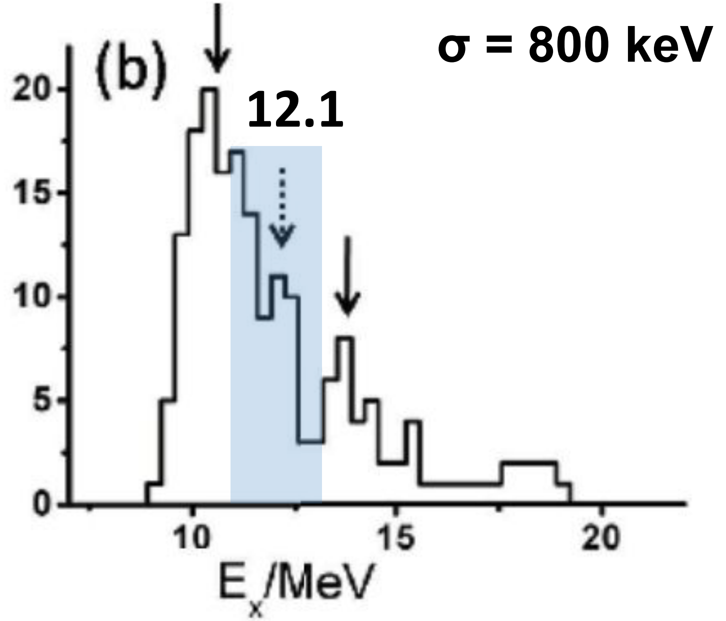


Yang et al. (2014)

# Angular distribution

## 11.9 MeV resonance

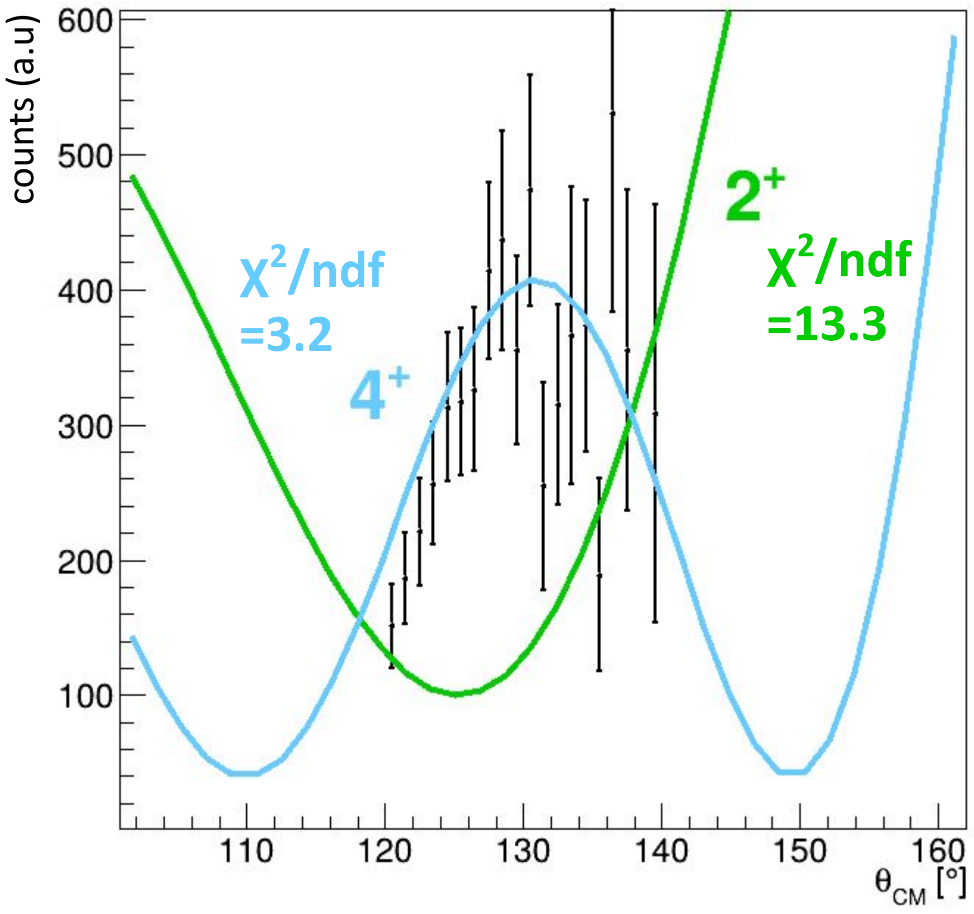


## 12.4 MeV resonance

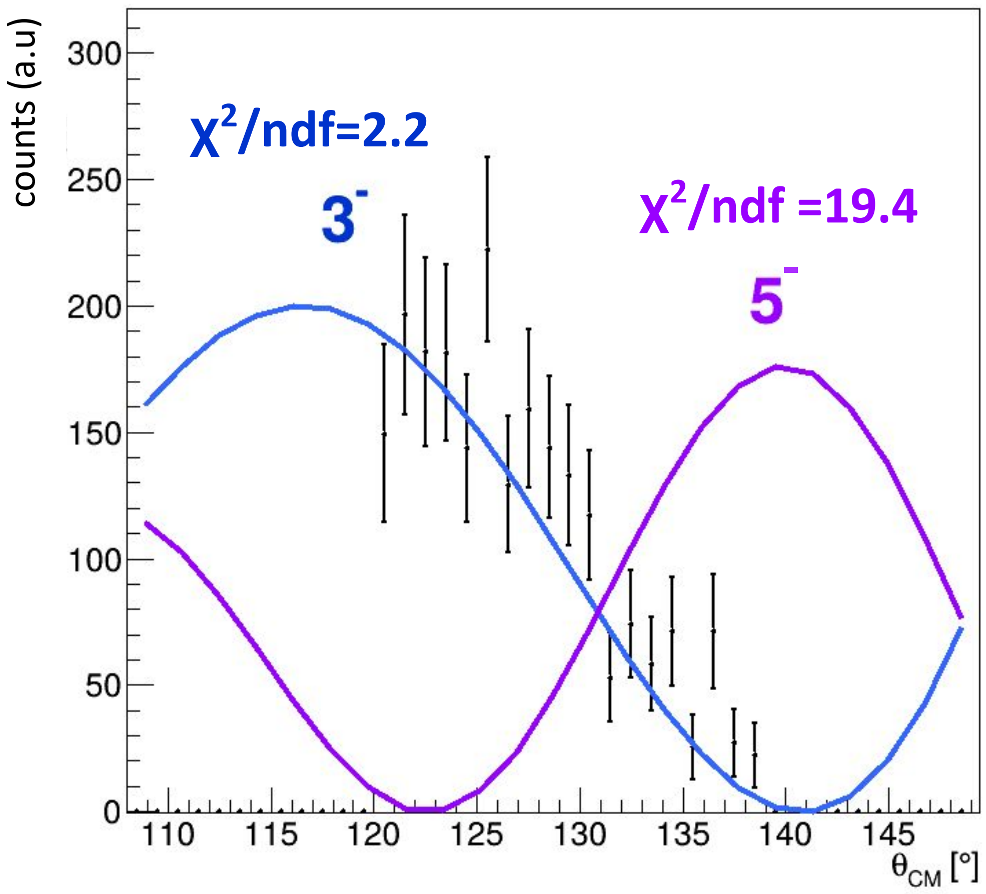

# R-Matrix fit

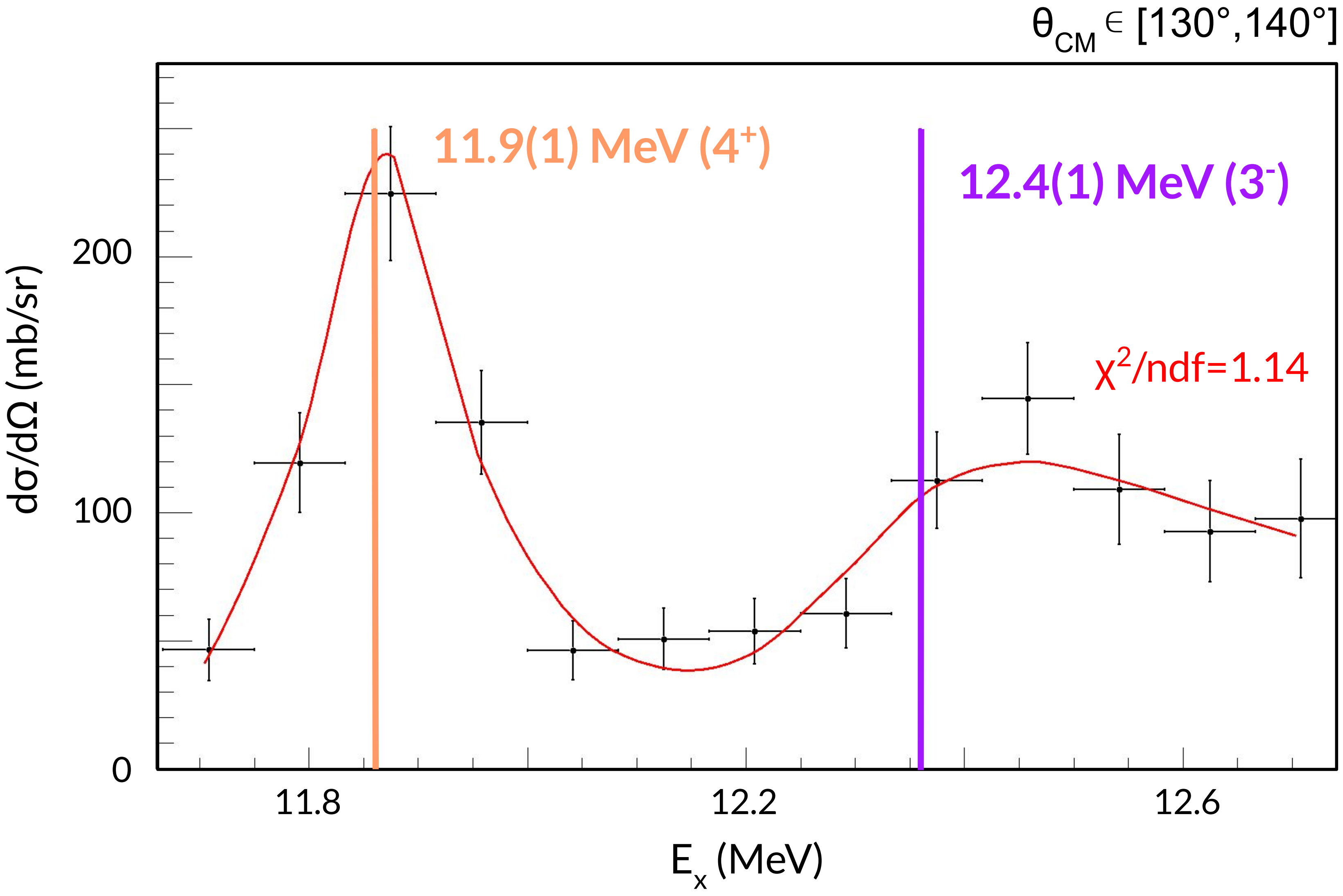
$\theta_{CM} \in [130°,140°]$
11.9(1) MeV (4+)
12.4(1) MeV (3-)
χ2/ndf=1.14
dσ/dΩ (mb/sr)
0
100
200
11.8
12.2
12.6
Ex (MeV)

# R-Matrix fit

only $^{4}He+^{8}He$ channel

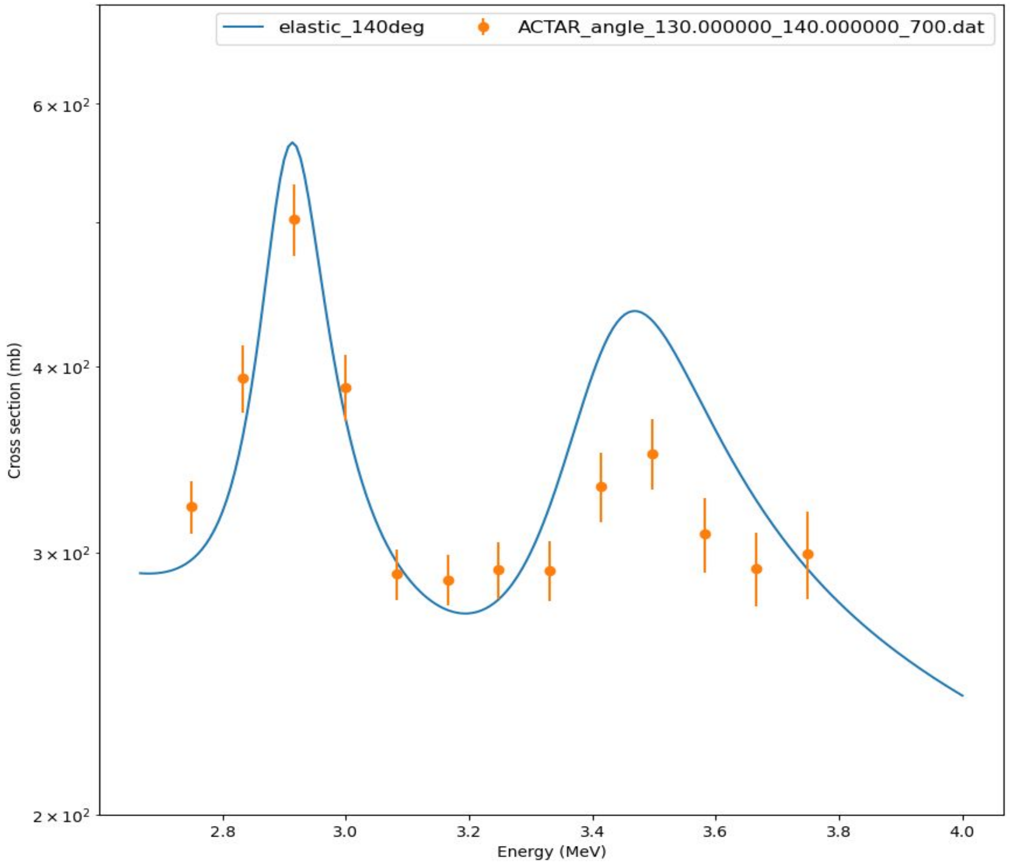


$^{4}He+^{8}He$, $^{6}He+^{6}He$, $^{11}Be+n$ and $^{10}Be+2n$ channels

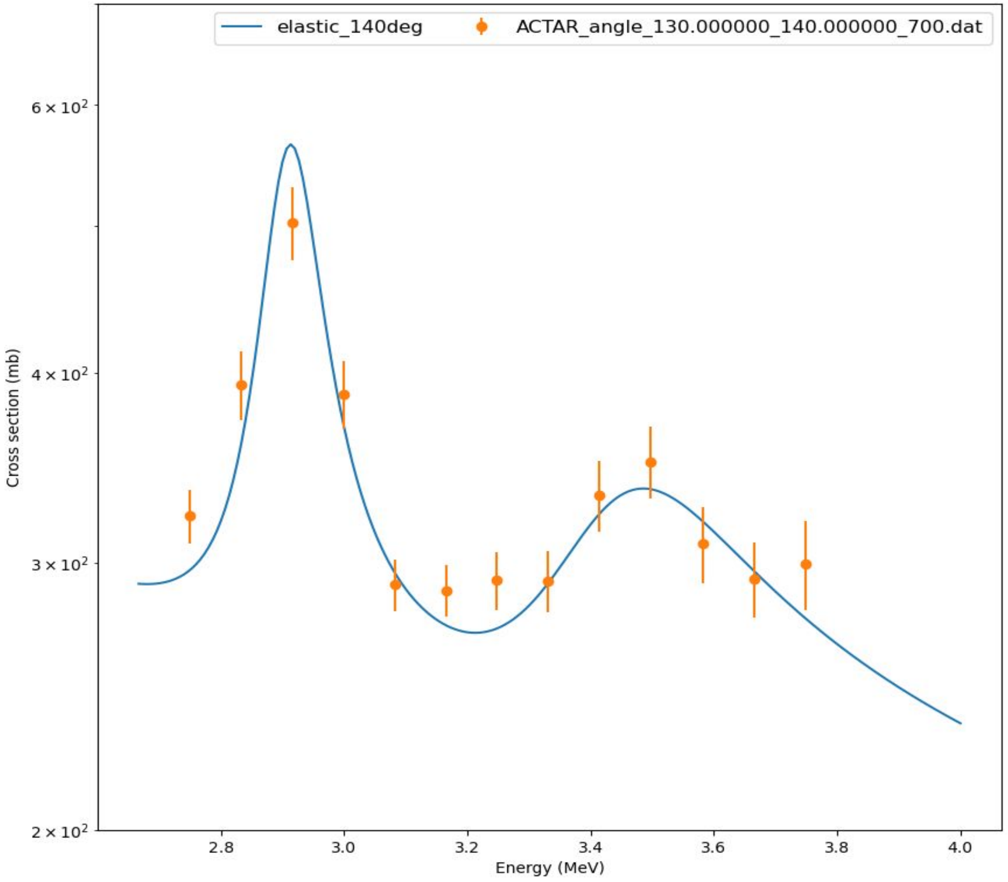

# R-Matrix fit

| Spin | 4+ | 3- |
|---|---|---|
| Ex [MeV] | 11.9(1) | 12.4(1) |
| $\Gamma(^4He+^8He)$ [keV] | 205(29) | 295(53) |
| $\Gamma(^6He+^6He)$ [keV] | 25(21) | 9(12) |
| $\Gamma(^{11}Be+n)$ [keV] | 24(19) | 100(18) |
| $\Gamma(^{10}Be+2n)$ [keV] | 5(2) | 26(13) |

# Dimensionless Reduced Widths (θ²)

The experimental width depends strongly on:

- Coulomb barrier
- Centrifugal barrier
- Resonance energy

Two states with **identical internal structure** can have very different Γ just because of barrier effects.

$\theta^2 \ll 1$ → weak cluster structure

$\theta^2 \sim 1$ → strong cluster structure

Experimental width extracted from the R-matrix fit

$$\theta^2 = \frac{\Gamma_{\text{exp}}}{\Gamma_{\text{sp}}}$$

Single-particle width

Penetrability factor (Coulomb + centrifugal barrier)

$$\Gamma_{\text{sp}} = 2\, P_\ell(E)\, \gamma_W^2$$

Wigner reduced width (theoretical maximum)

# $\theta^2$ of different channels : $4^+$ state

- 11.9 MeV - $4^+$ :

| channel | $\theta^2$ |
|---|---|
| $^4He+^8He$ | 0.86(12) |
| $^6He+^6He$ | 0.24(20) |
| $^{11}Be+n$ | 0.001(1) |

- dominant $^4He$ + $^8He$ structure
- minor $^6He+^6He$ mixing

# $\theta^2$ of different channels: $3^-$ state

- 12.4 MeV - $3^-$ :

| channel | $\theta^2$ |
|---|---|
| $^4He+^8He$ | 0.21(2) |
| $^6He+^6He$ | 0.02(3) |
| $^{11}Be+n$ | 0.01(1) |

$\sum\theta^2<1$ → possible missing channel

# $\theta^2$ of different channels: $3^-$ state

- 12.4 MeV - $3^-$ :

| channel | $\theta^2$ |
|---|---|
| $^4He+^8He$ | 0.21(2) |
| $^6He+^6He$ | 0.02(3) |
| $^{11}Be+n$ | 0.01(1) |
| $^5He+^7He$ | 0.88(30) |
| $^8Be+4n$ | 0.49(40) |

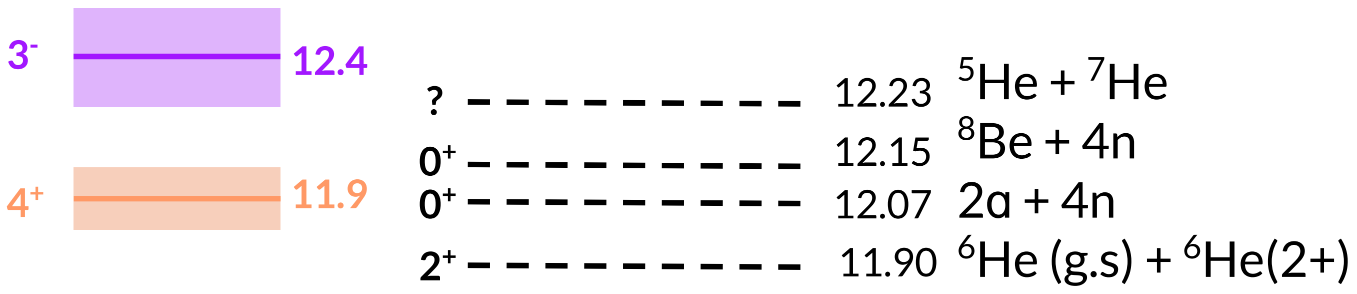


- **$^5He(3/2^-)+^7He(3/2^-)$:** $3^-$ obtained with **L=1**
- **$^8Be(0^+)+4n$:** $3^-$ requires **L=3**
  (L=3 for all the other channels)

→ Lower orbital momentum favors **$^5He+^7He$** cluster structure.

# Comparison with theory and Outlook

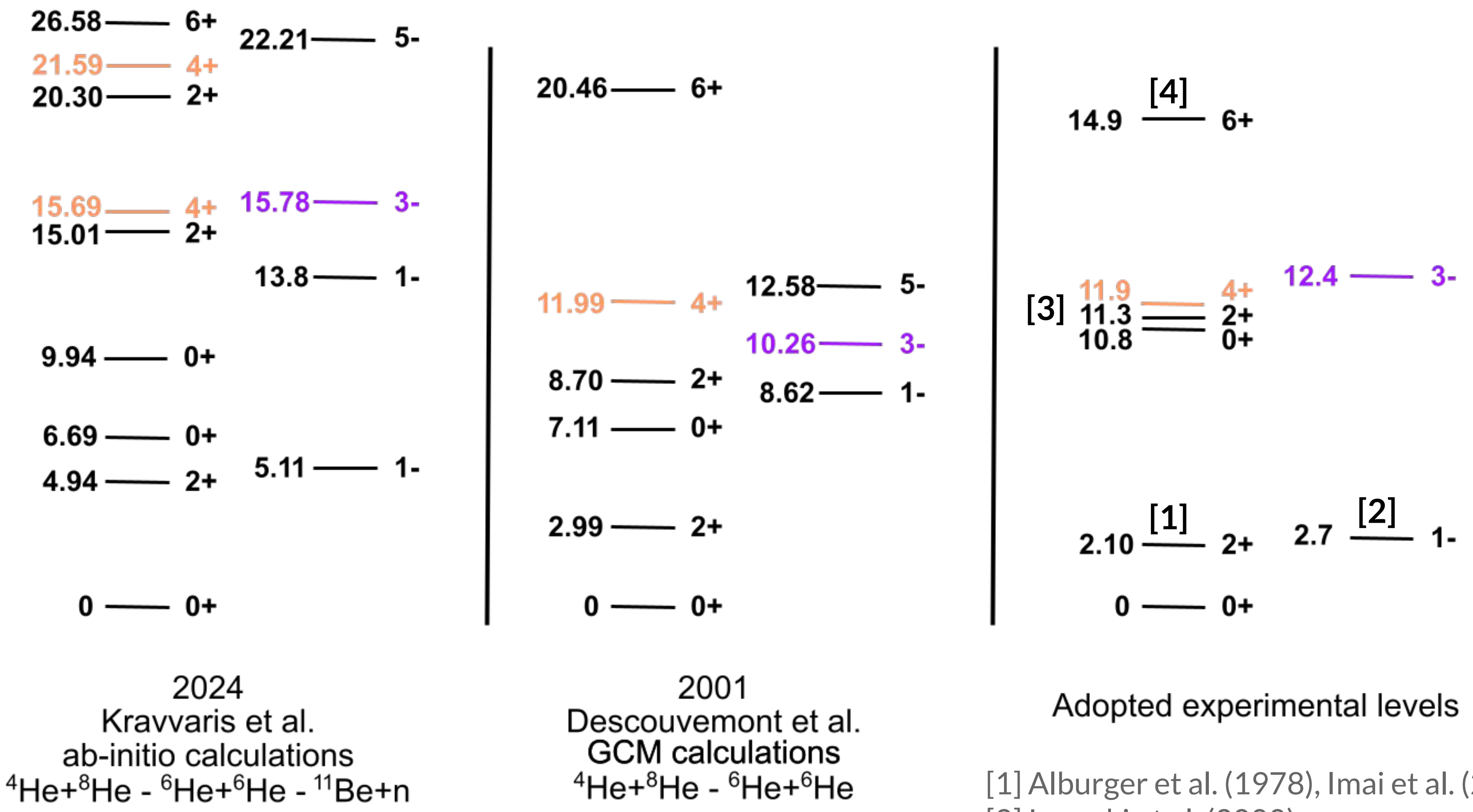


[1] Alburger et al. (1978), Imai et al. (2009)
[2] Iwasaki et al. (2000)
[3] Freer et al. (1999), Saito et al. (2007)
[4] Freer et al. (1999), Freer et al. (2001)

Outlook :

- future Gamow Shell Model calculation* with $^5$He+$^7$He
- experiment to measure $^5$He+$^7$He ($^4$He + $^6$He + 2n)

* Nicolas Michel, Marek Ploszajczak

# Conclusion

11.9 MeV - $4^+$ :

- Compatible with 12.1 MeV ($2^+$) by *Yang et al.* but ≠ spin assignment
- Compatible with states predicted by *Descouvemont et al. (GCM)* and *Kanada-En'yo et al. (AMD)*
- strong $^4$He+$^8$He molecular structure
- mixing with $^6$He+$^6$He

12.4 MeV - $3^-$ :

- Not yet measured, predicted at different energies
- Candidate for $^5$He+$^7$He exotic molecular structure

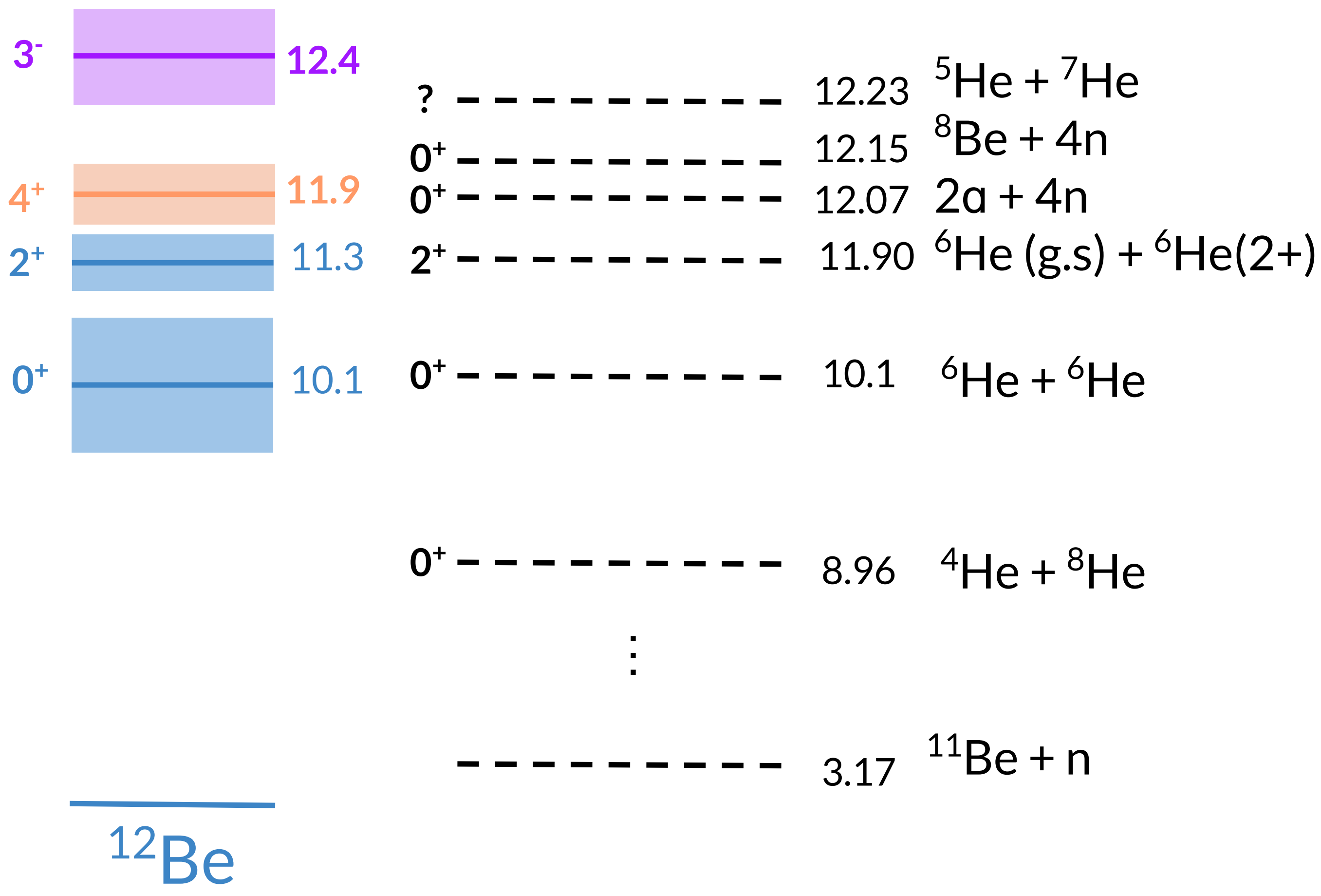

# Collaboration

# Thank you for your attention !

**Spokespersons:**

- Valdir Guimarães - University of São Paulo - Brazil
- Thomas Roger - GANIL - France

**GANIL, France :** F. de Oliveira, T. Roger, J. Pancin, C. Nicolle, M. Fisichella, L. Dienis, A. Cassisa, M. Le Joubioux, J. C. Thomas, B. Jacquot, A. Navin, N. Michel, M. Ploszajczak
**USC, Spain** : B. Fernandez-Dominguez, M. Lozano González, B. Errandonea Félix
**CEA, France :** C. Fougères, M. Vandebrouck
**INFN-Sezione di Catania, Italy :** M. Grazia Pellegriti
**University of Huelva, Spain :** A. Miguel Sánchez Benitez
**VINCA, Yugoslavia :** T. Milanovic, I. Celikovic
**IFIN-HH, Bucharest, Romania :** M. Stanoiu
**NPI ASCR Rez, Czech Republic :** J. Mrazek
**Michigan State University, USA :** J. C. Zamora
**NSCL-MSU, USA :** Y. Ayyad
**IBS (CENS), South Korea :** X. Pereira Lopes

# Backup slides

# $\theta^2$ of different channels : $4^+$ state

- 11.9 MeV - $4^+$ :

| channel | $\theta^2$ |
|---|---|
| $^4He+^8He$ | 0.86(12) |
| $^6He+^6He$ | 0.24(20) |
| $^{11}Be+n$ | 0.001(1) |

→ No $^6He$ from the $^6He+^6He$ channel is observed in the data. Maximum undetected $\theta^2$ in ACTAR TPC: **0.28**

- dominant $^4He + ^8He$ structure
- minor $^6He+^6He$ mixing

# Resonant elastic scattering

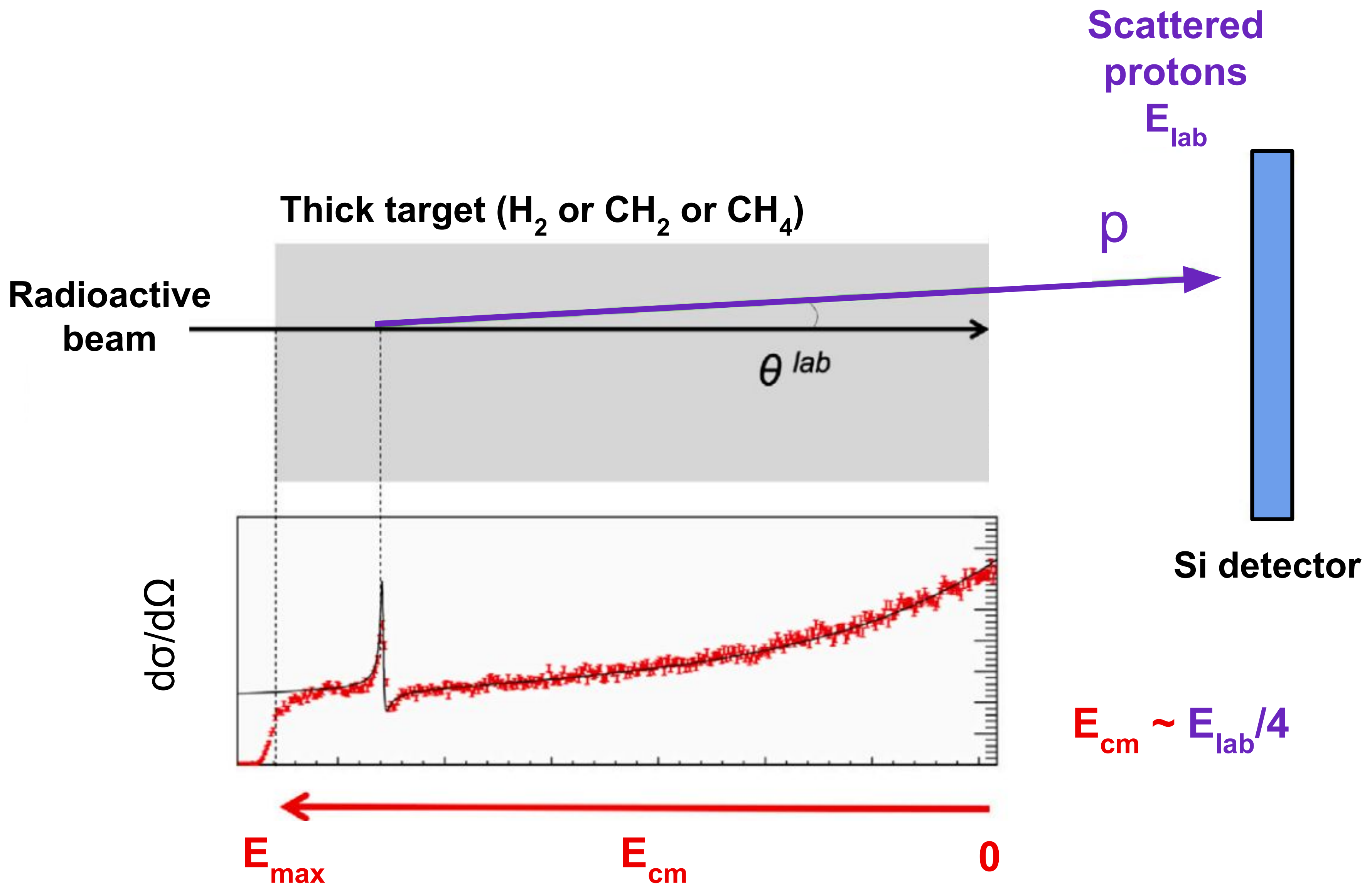

# Analysis : tracks reconstruction

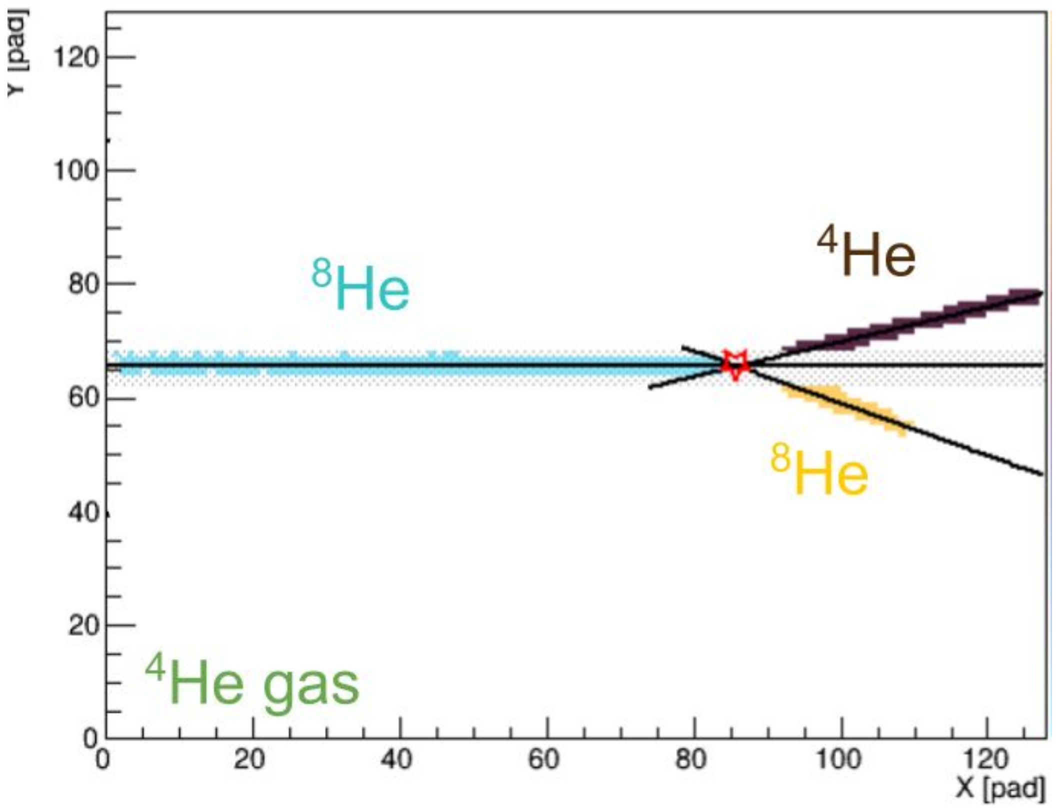


## CLIMB Algorithm

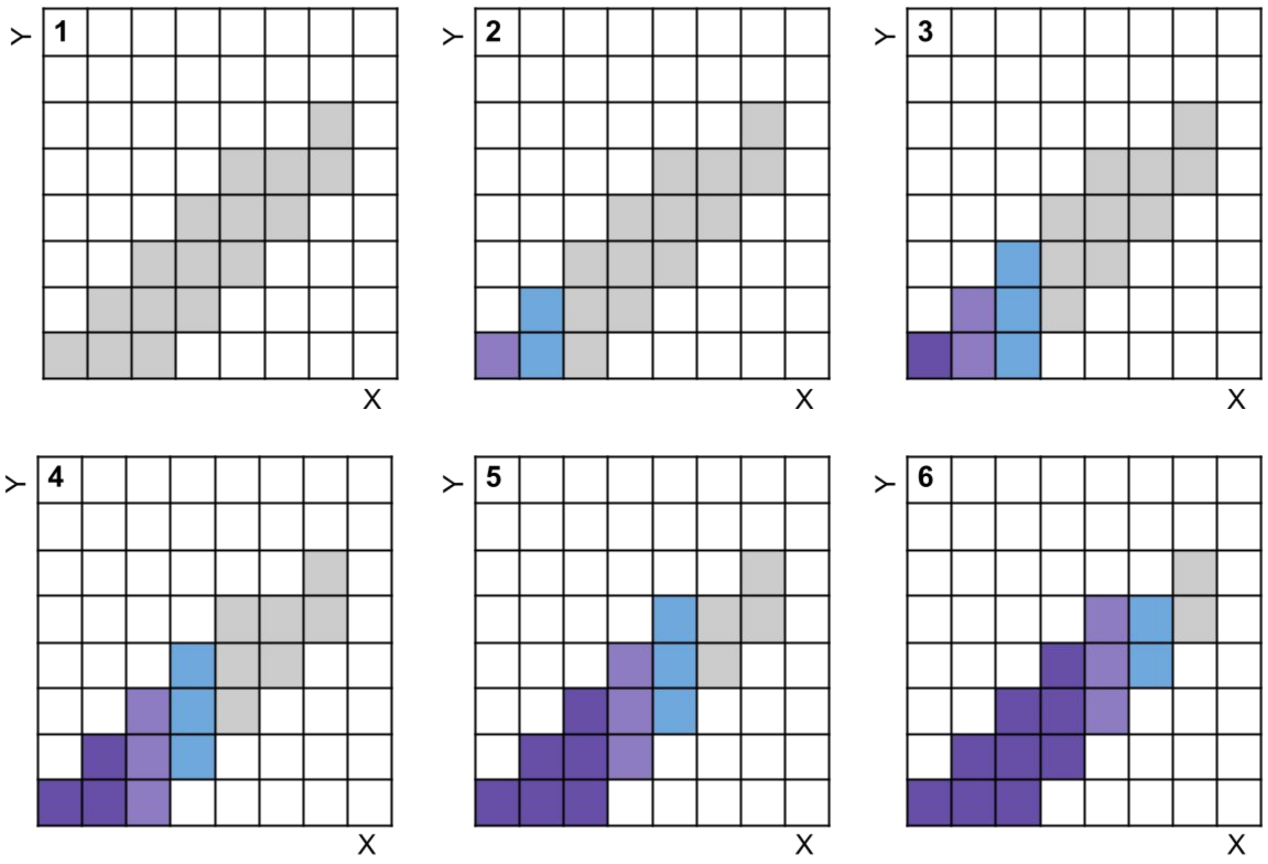

# Analysis : tracks reconstruction

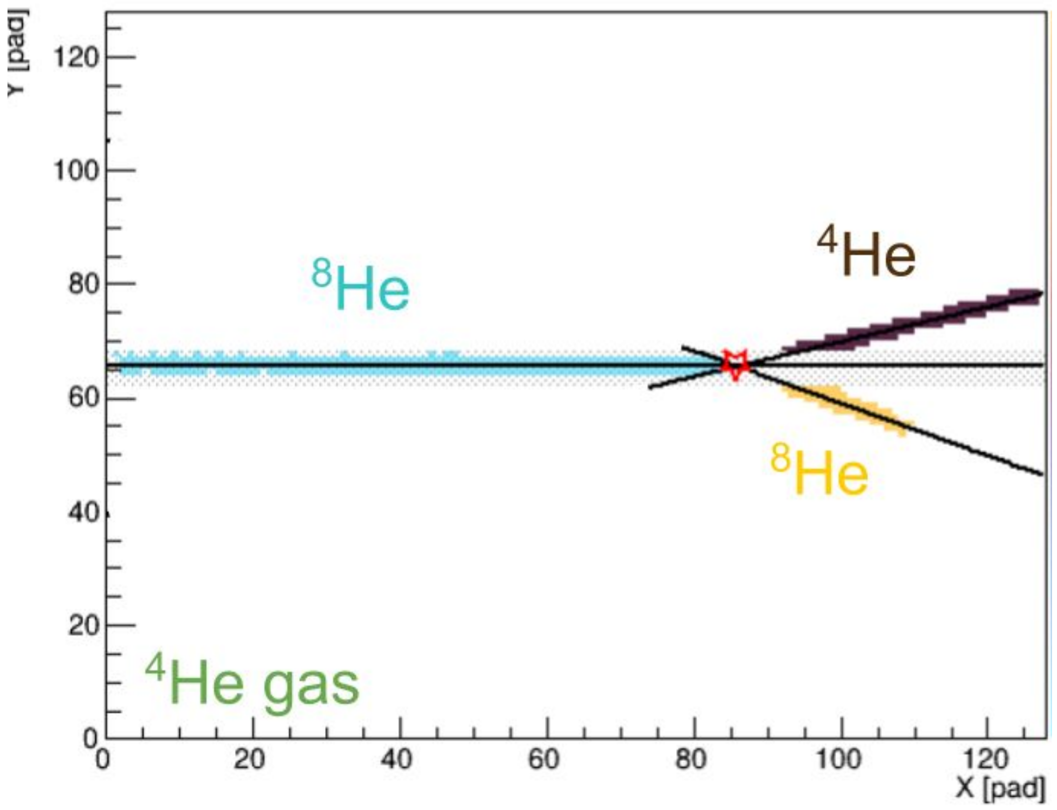


## CLIMB Algorithm

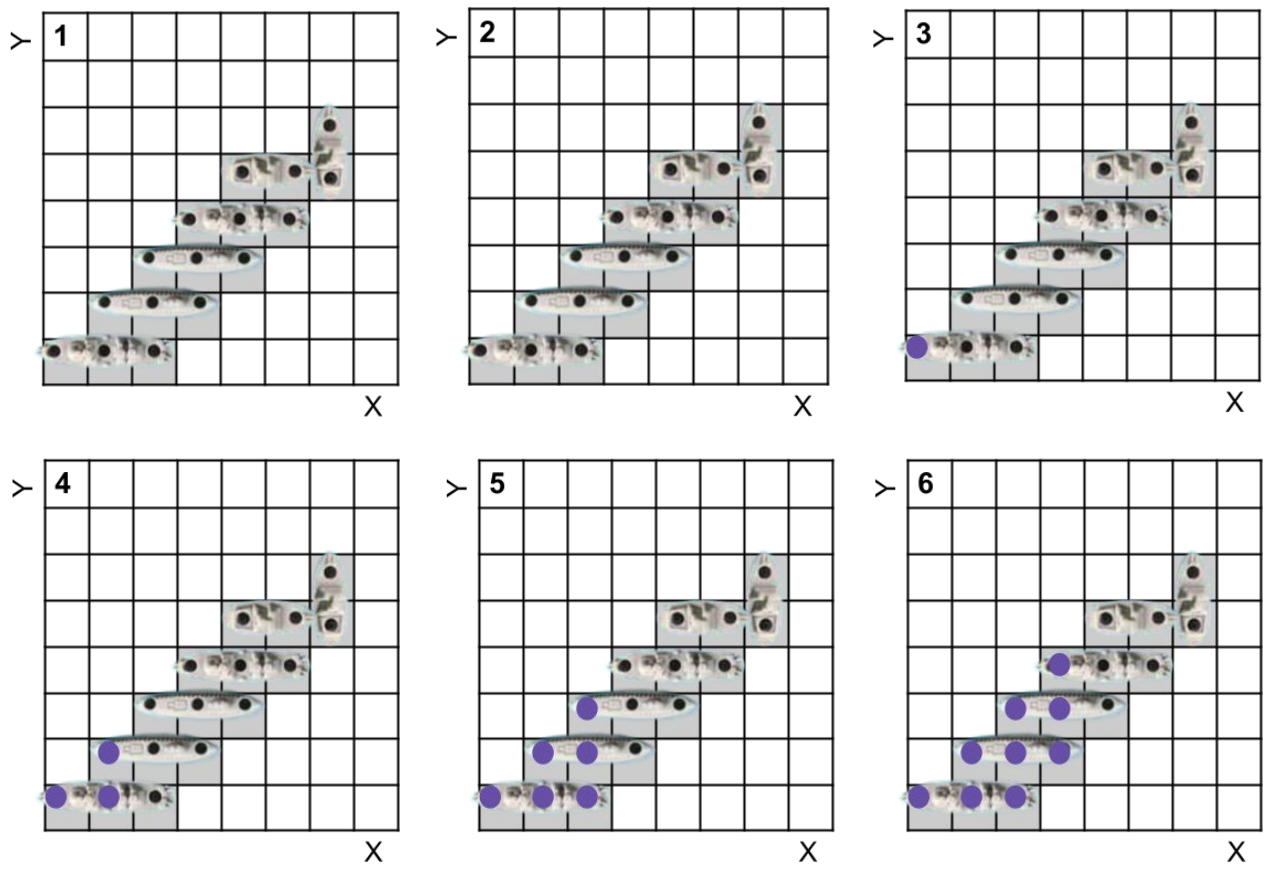


↩

# Selection on charge profile

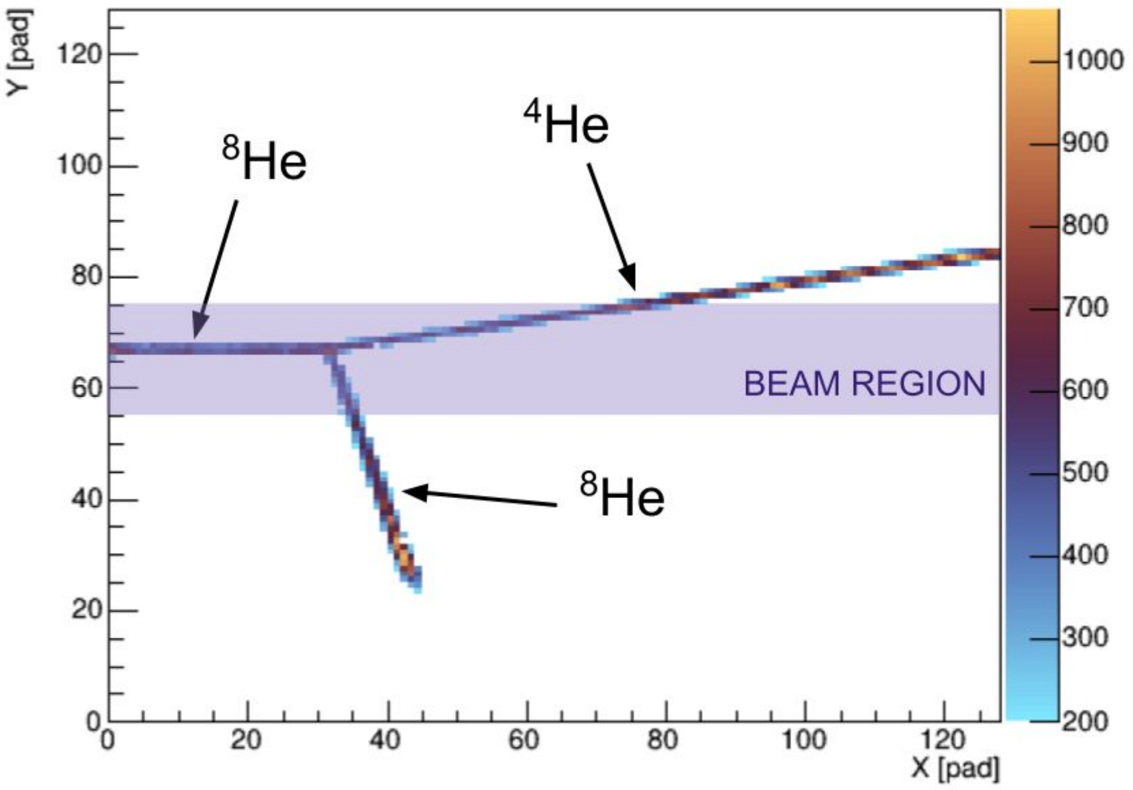


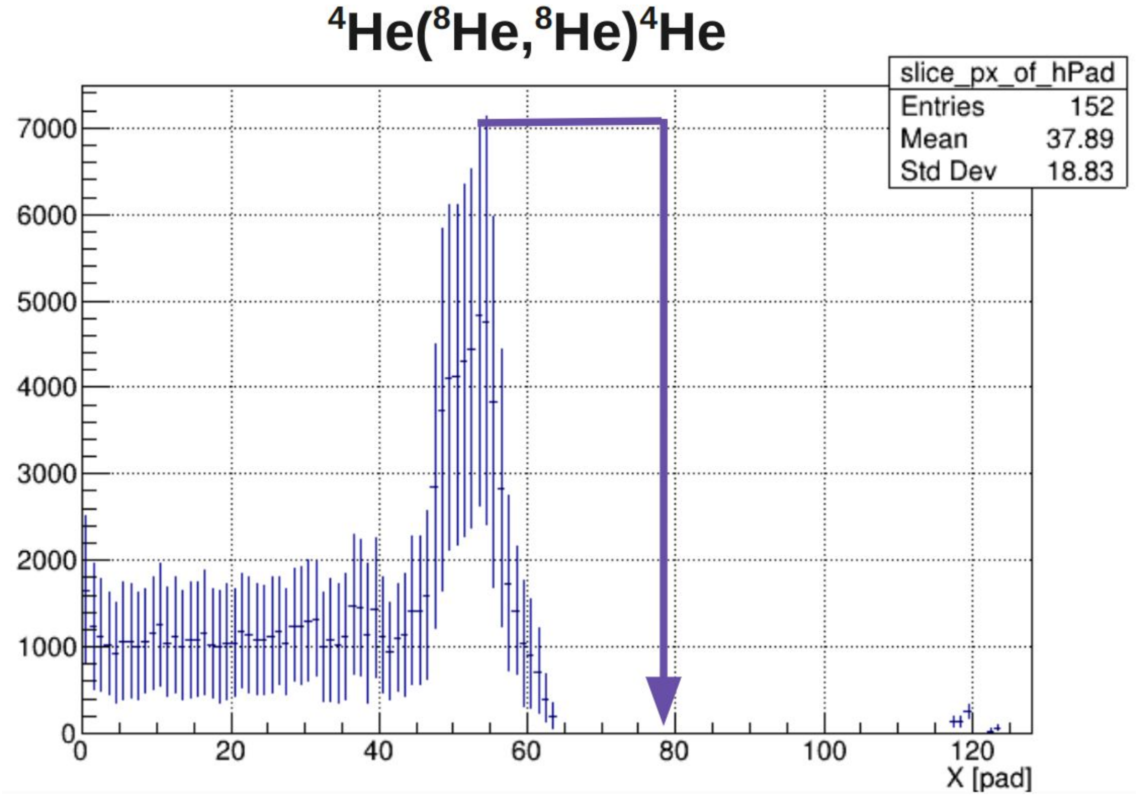


↩

# Selection on charge profile

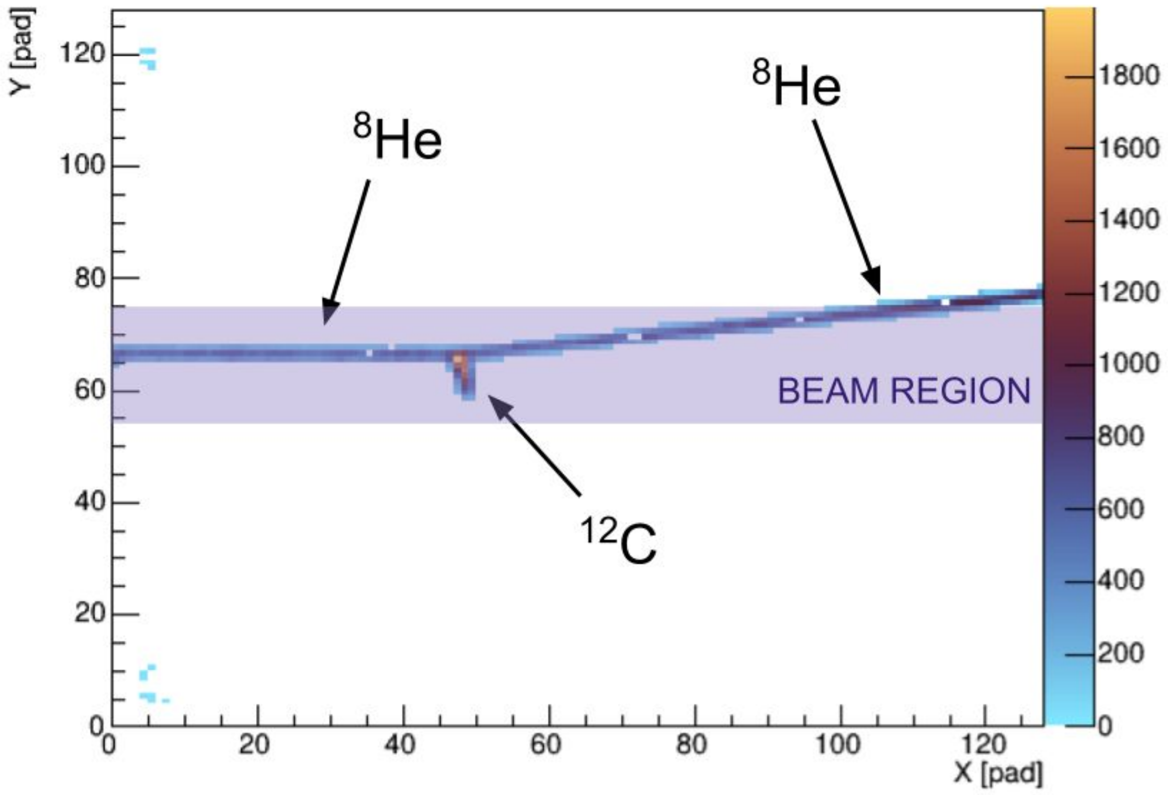


$^{12}$C($^8$He,$^8$He)$^{12}$C

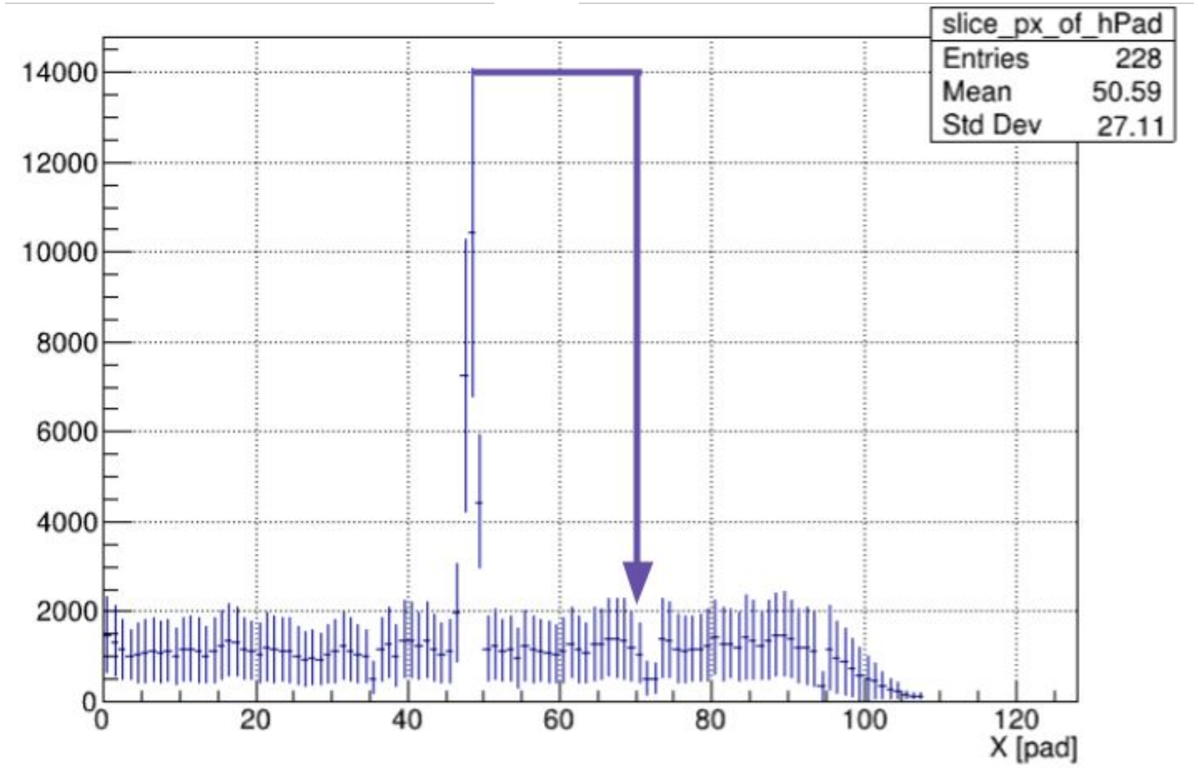


↩

# Selection on the angular correlations

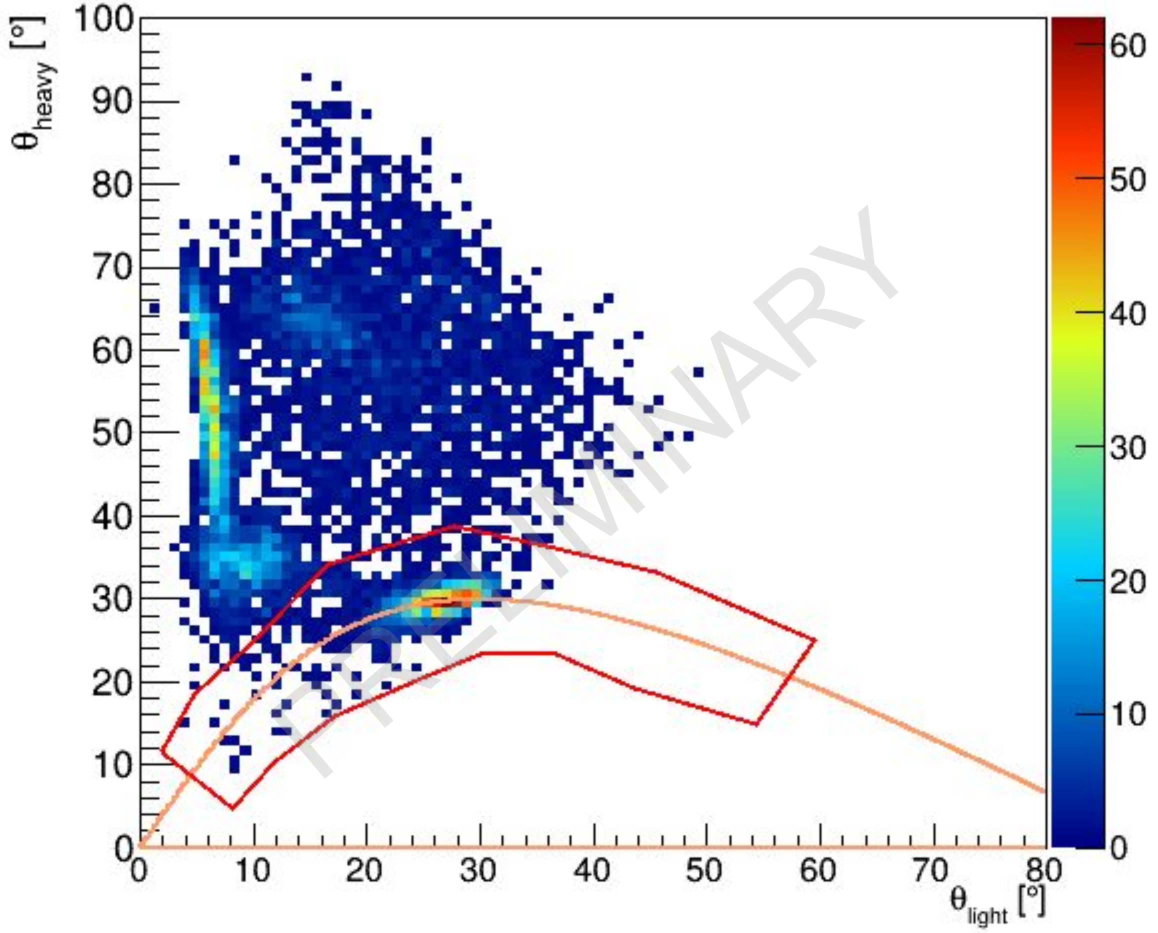


↩

# Comparing Elight from beam track vs light track + Si

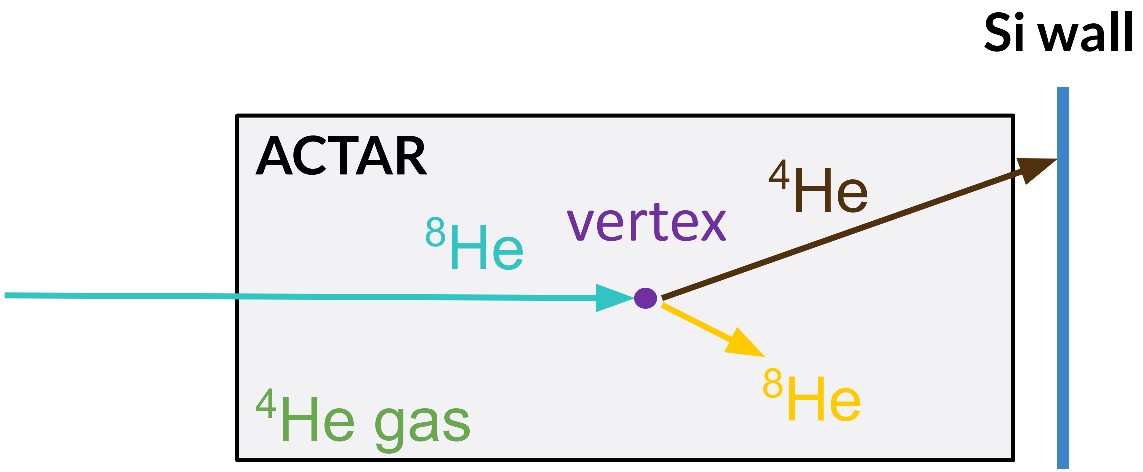


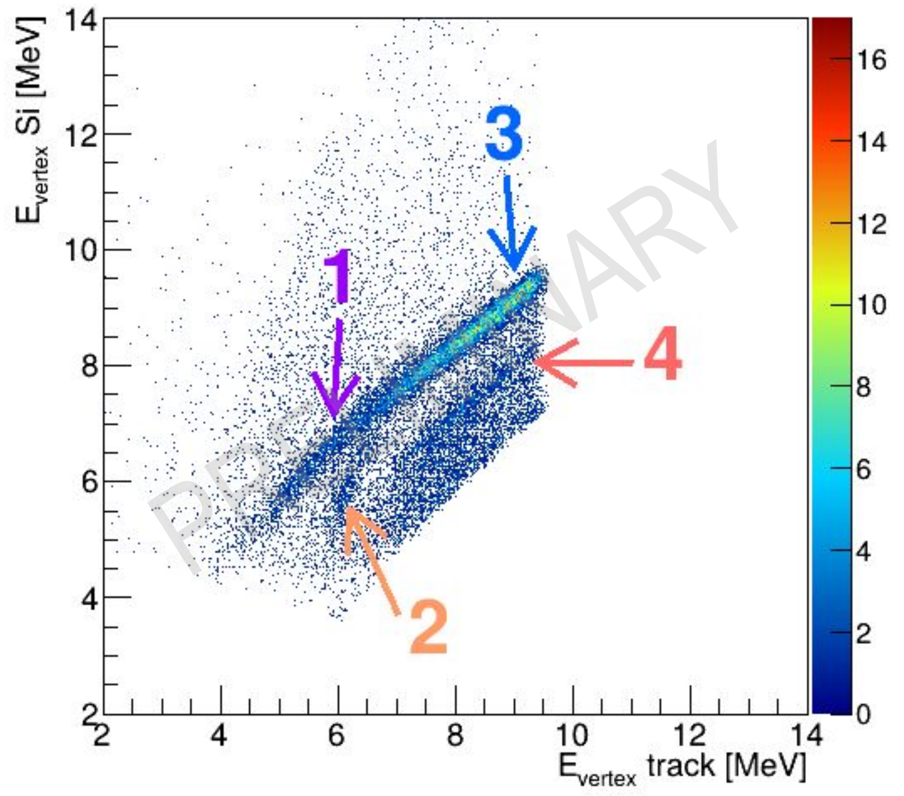

# Comparing Elight from beam track vs light track + Si

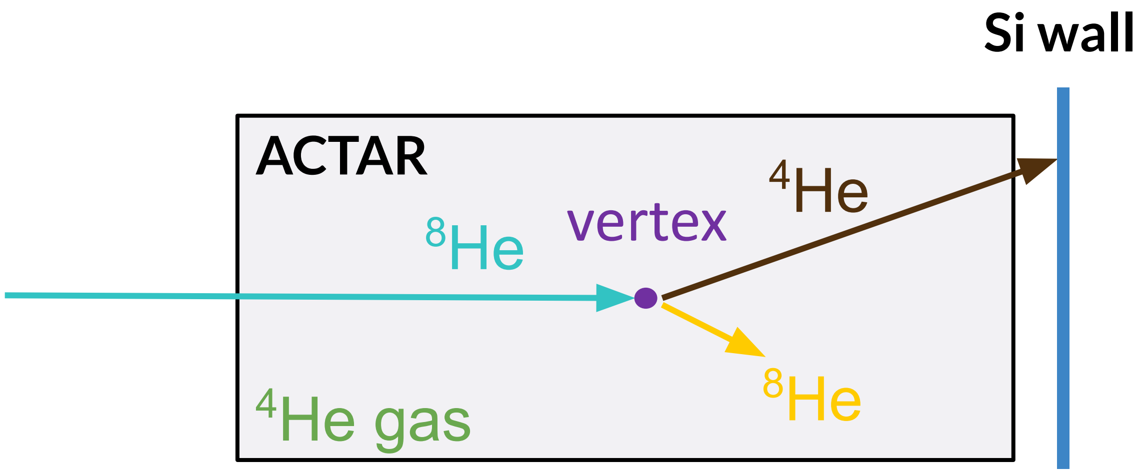


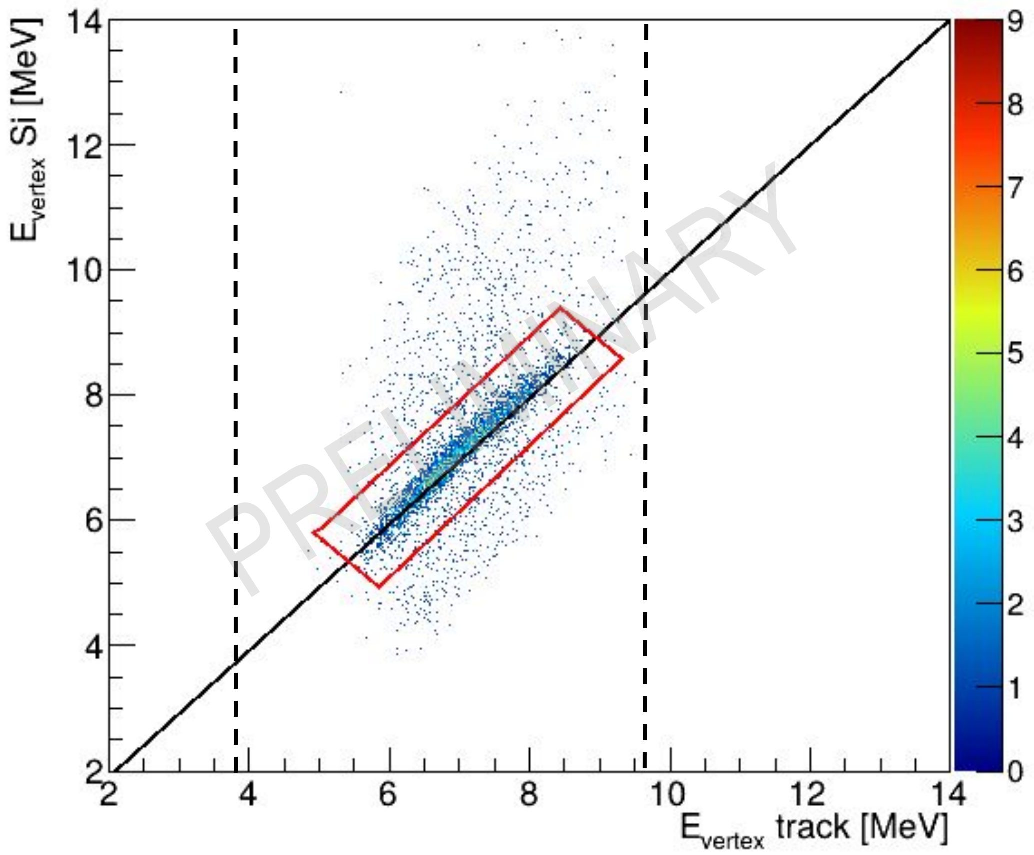


↩

# Excitation energy reconstruction

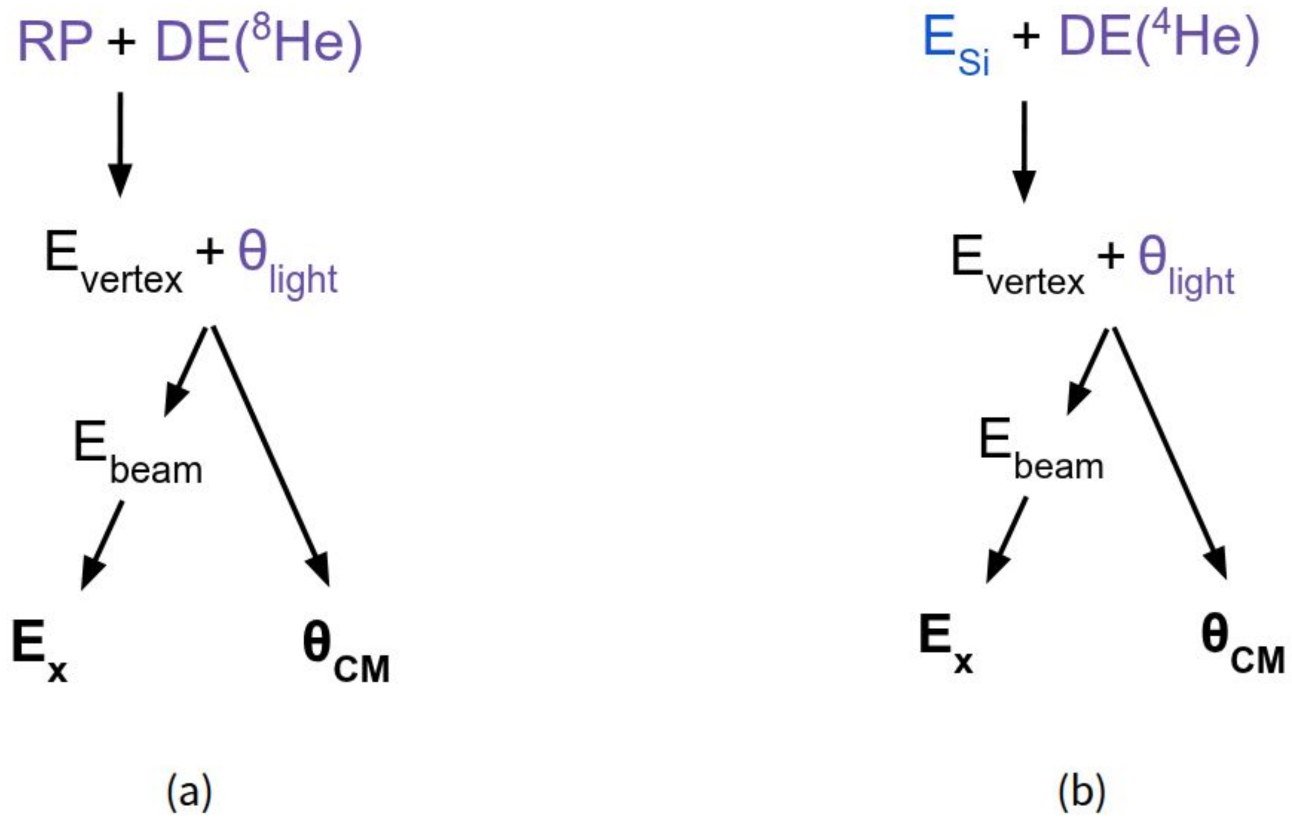


Figure II.46: Reconstruction diagram of $E_x$ and $\theta_{CM}$. The parameters in purple, RP, DE and $\theta_{light}$ are reconstructed from the tracks in ACTAR TPC. RP is the reaction point and DE the energy loss in ACTAR TPC. The parameter in blue is measured in the silicon detectors (a) Reconstruction using the reaction point (b) Reconstruction using the silicon energy.

# Excitation energy reconstruction

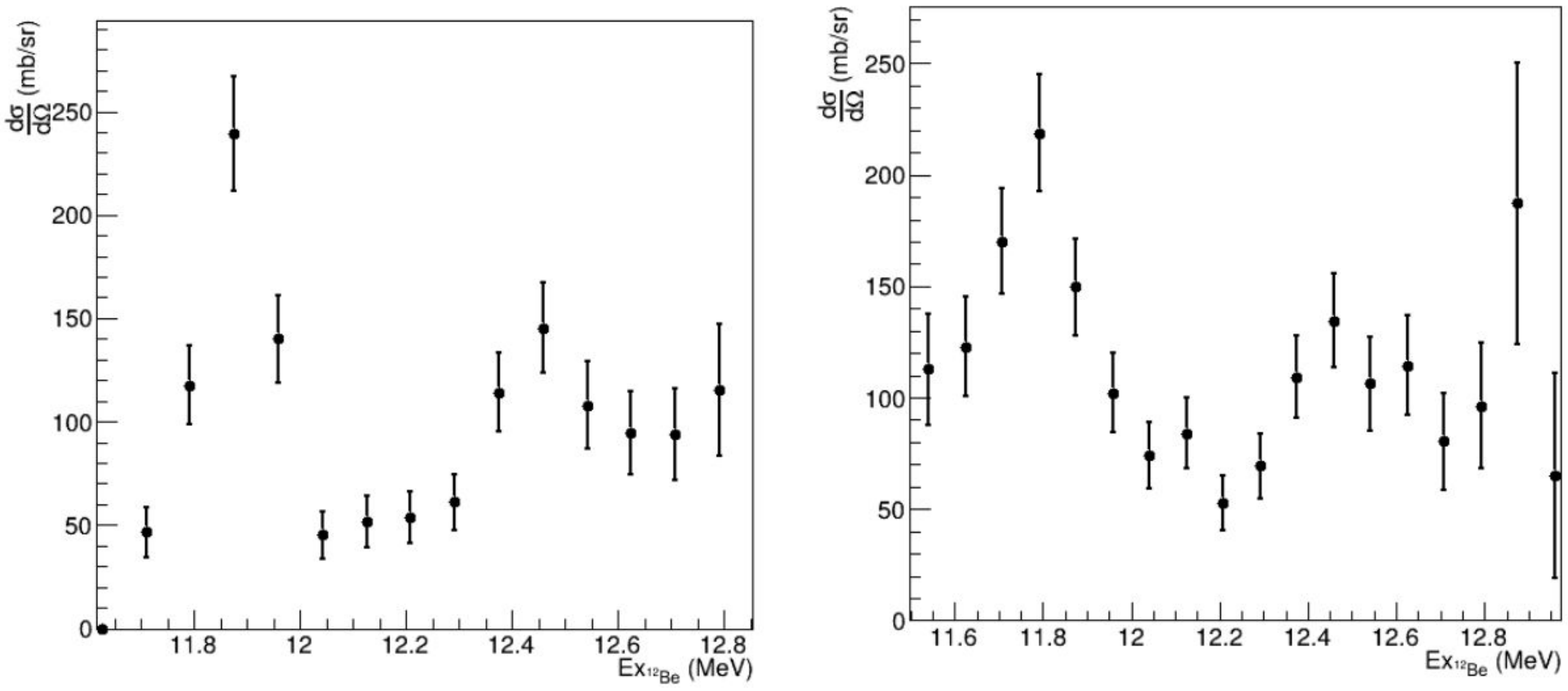


(a) (b)

Figure II.47: Excitation energy of $^{12}$Be, projection from angle 130 to 140°, ACTAR TPC filled with 700 mbar of gas. (a) Excitation energy reconstructed from the reaction point in ACTAR TPC. (b) Excitation energy reconstructed from the silicon energy.

# Energy resolution

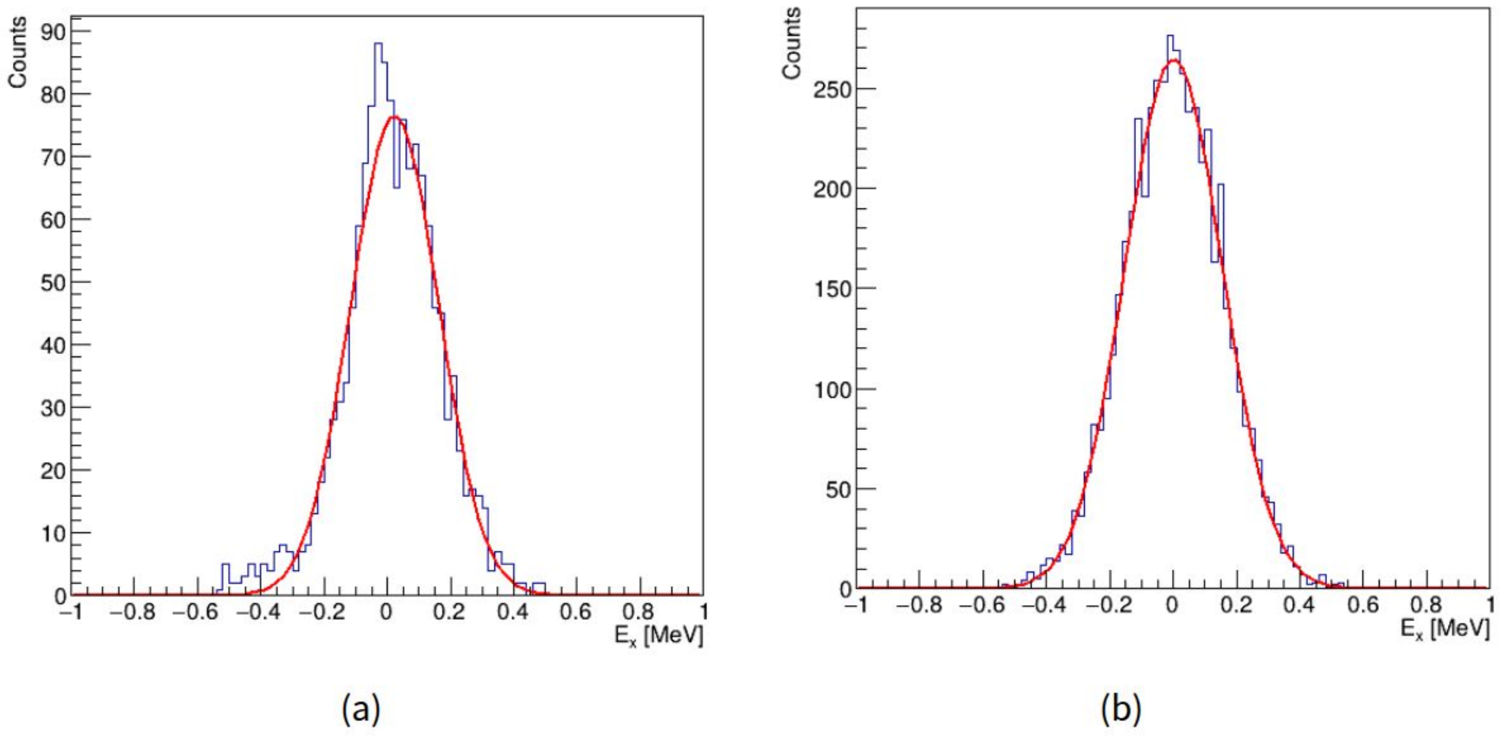


Figure II.51: Excitation energy of the scattered $^{8}$He in MeV. (a) Experimental data for 700 mbar in ACTAR TPC after background removal. (b) Simulation obtained with $\sigma(Si) = 50$ keV, $\sigma(\theta) = 0.40$ rad, and $\sigma(e_{\text{beam}}) = 250 \pm 10$ keV.

From equation II.17, we deduce the resolution of the excitation energy of $^{12}$Be:

$$\sigma(E^*_{^{12}Be}) = \sigma(e_{beam}) \times \frac{m_{^4He}}{m_{^4He} + m_{^8He}} = 83 \pm 3 \text{ keV}. \quad \text{(II.18)}$$

↩

# Energy resolution

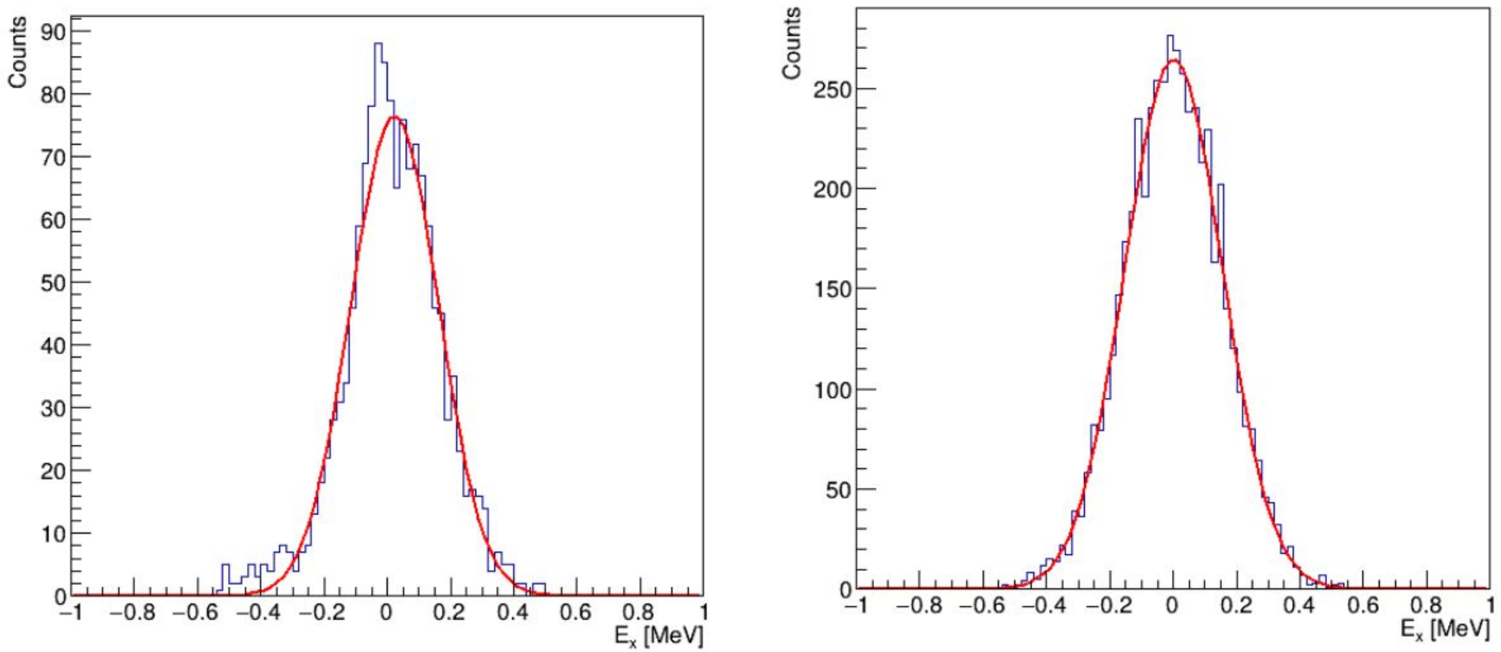


(a) (b)

Figure II.51: Excitation energy of the scattered $^{8}$He in MeV. (a) Experimental data for 700 mbar in ACTAR TPC after background removal. (b) Simulation obtained with $\sigma(Si) = 50$ keV, $\sigma(\theta) = 0.40$ rad, and $\sigma(e_{\text{beam}}) = 250 \pm 10$ keV.

From equation II.17, we deduce the resolution of the excitation energy of $^{12}$Be:

$$\sigma(E^{*}_{^{12}Be}) = \sigma(e_{beam}) \times \frac{m_{^4He}}{m_{^4He} + m_{^8He}} = 83 \pm 3 \text{ keV}. \qquad \text{(II.18)}$$

# Angular distribution

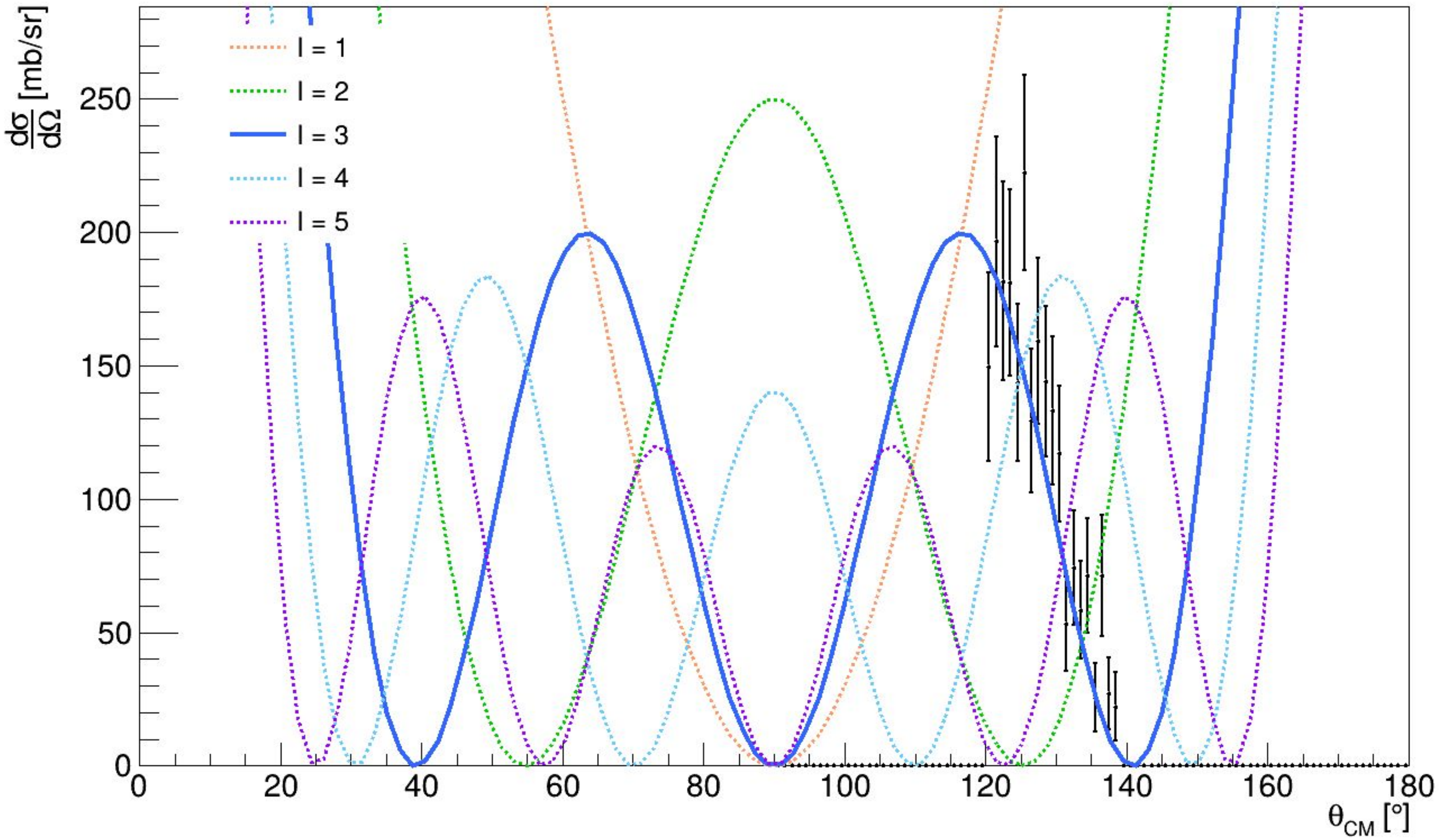


↩

# Angular distribution

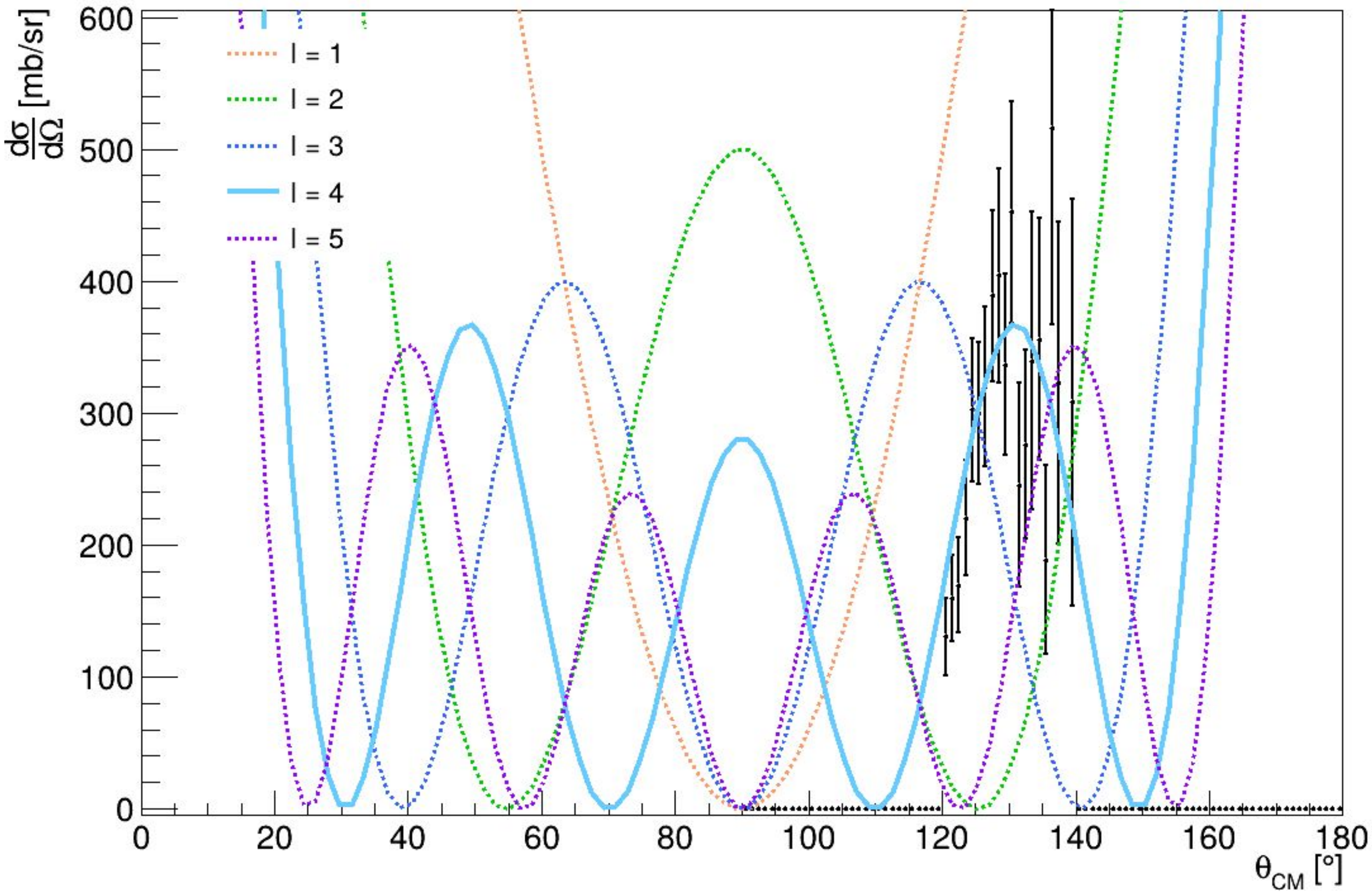


↩

# Bayesian analysis

Bayesian R-matrix Inference Code Kit (BRICK [1]) published in 2021

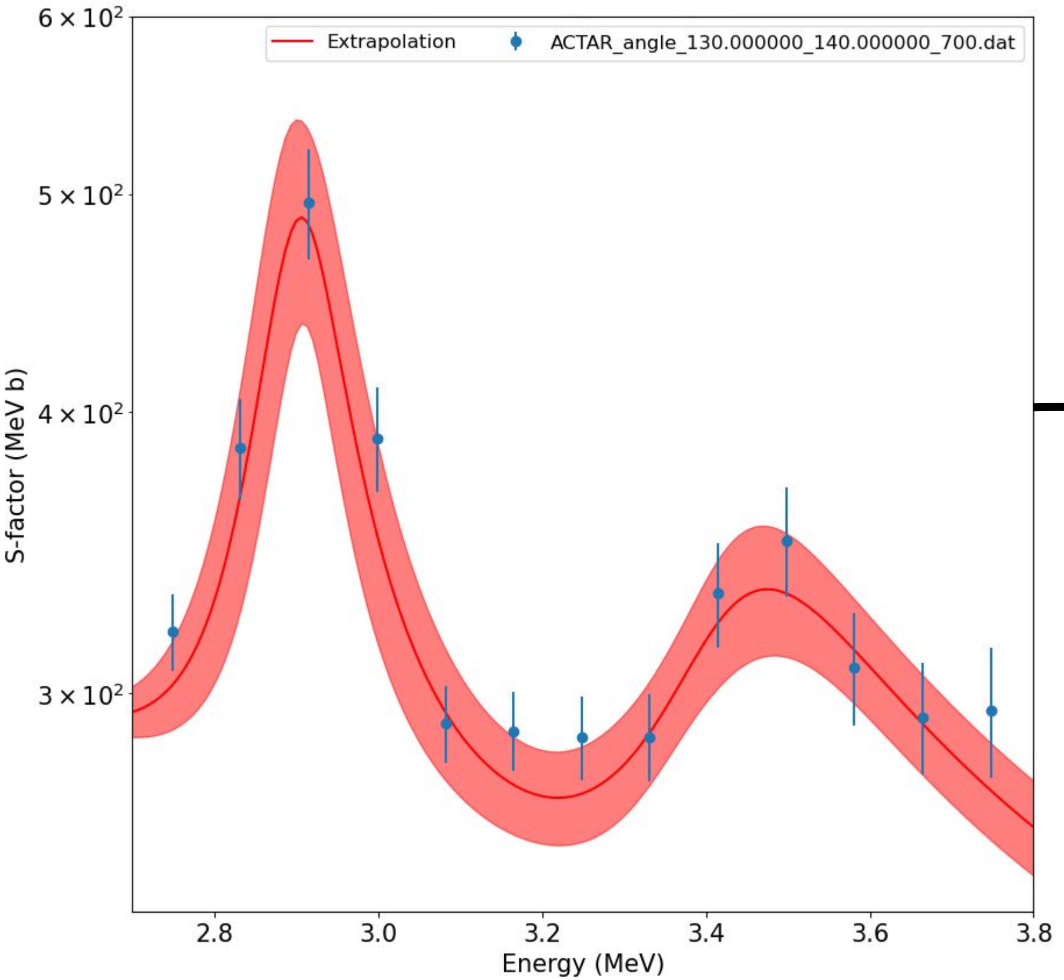


| Spin | 4+ | 3- |
| --- | --- | --- |
| Ex [MeV] | 11.9(1) | 12.4(1) |
| $\Gamma(^{4}He+^{8}He)$ [keV] | 205(29) | 295(53) |
| $\Gamma(^{6}He+^{6}He)$ [keV] | 25(21) | 9(12) |
| $\Gamma(^{11}Be+n)$ [keV] | 24(19) | 100(18) |
| $\Gamma(^{10}Be+2n)$ [keV] | 5(2) | 26(13) |

[1] https://github.com/odell/brick.git

# 5He+7He measurement

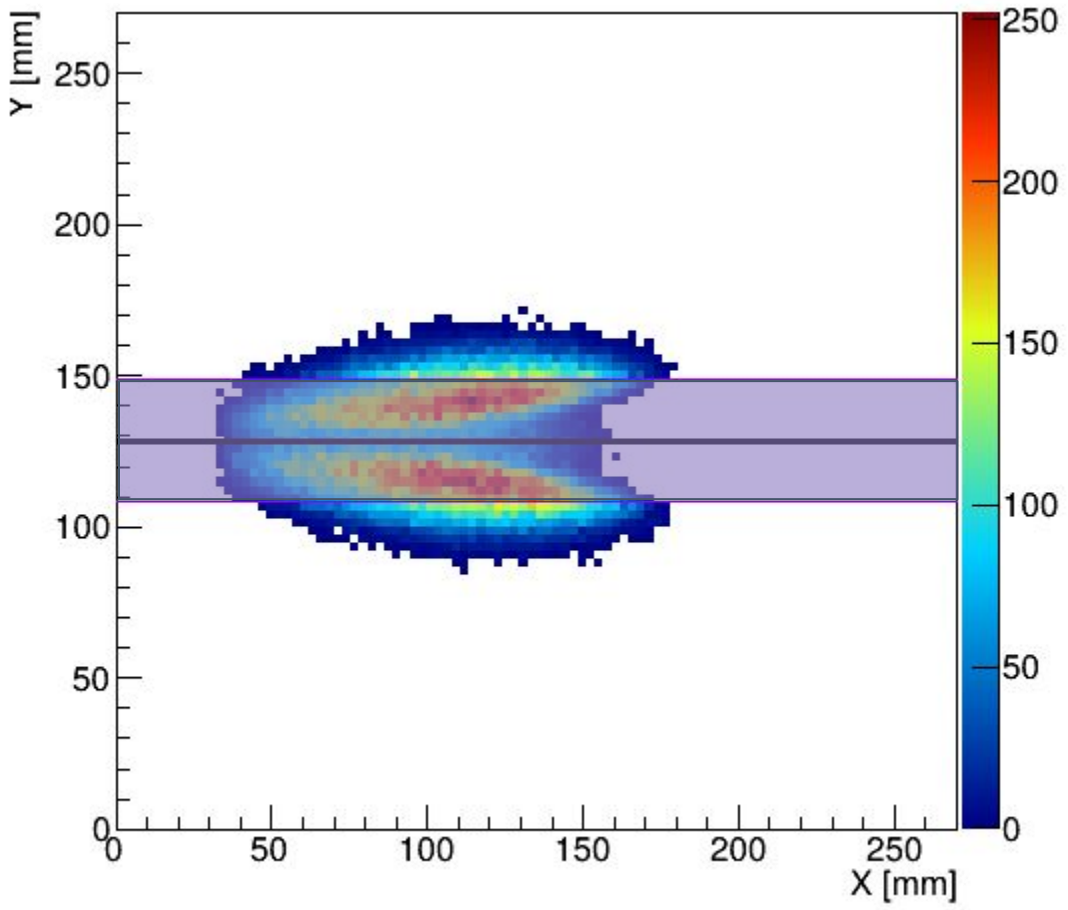


theoretically 10 possible measured counts but :

- $^{5}He$+$^{7}He$ (4He + 6He + 2n)
- Only 22% of events can launch a trigger
- Among a lot of contamination events and only 1% of events recorded

-> very few chance to see one $^{5}He$+$^{7}He$, none found in the data

↩

# 5He+7He measurement

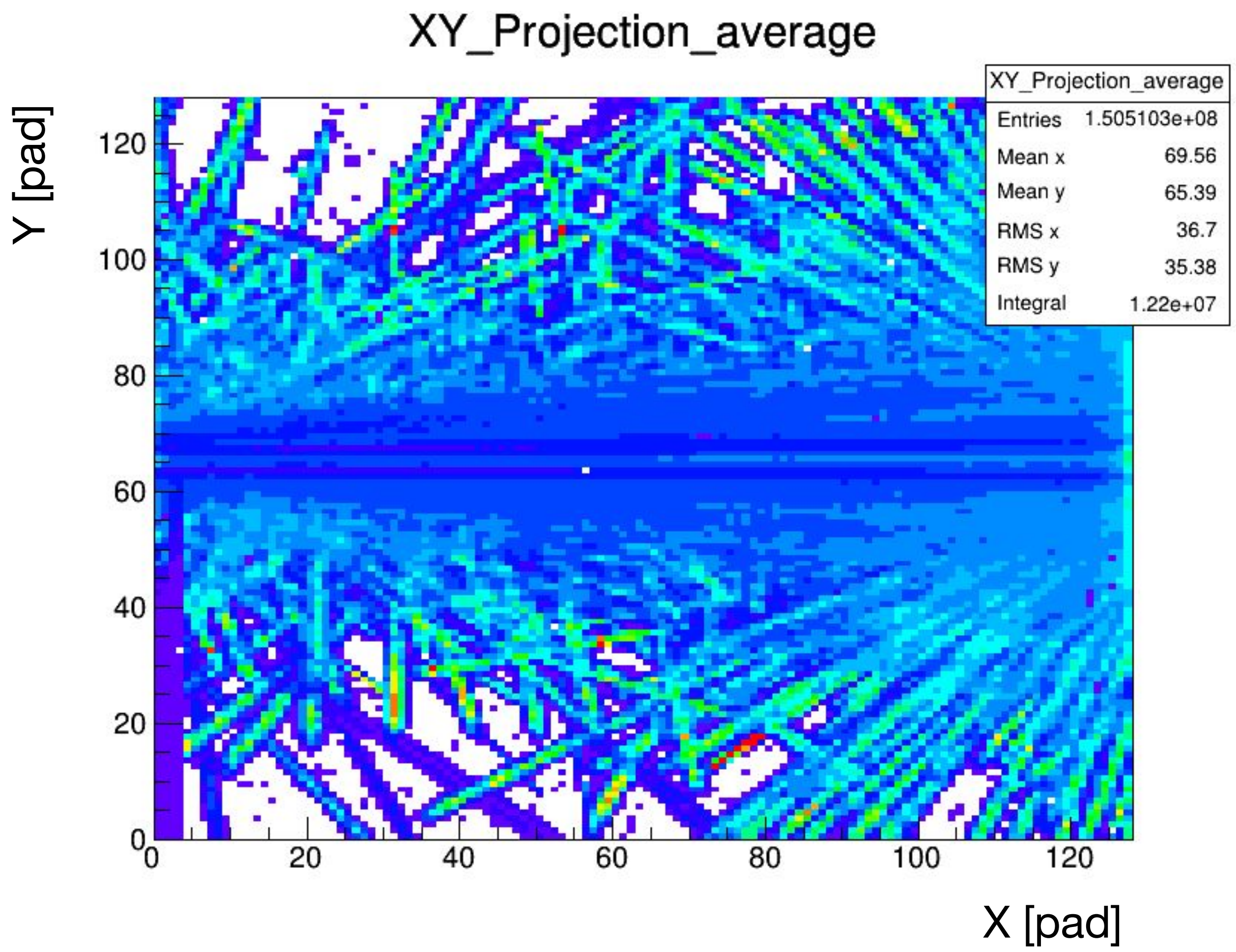


- $^{8}He$->$^{8}Li$->$^{8}Be$->2a
- Only 1% of ACTAR pad event recorded

↩

# R-Matrix fit

only $^{4}He+^{8}He$ channel

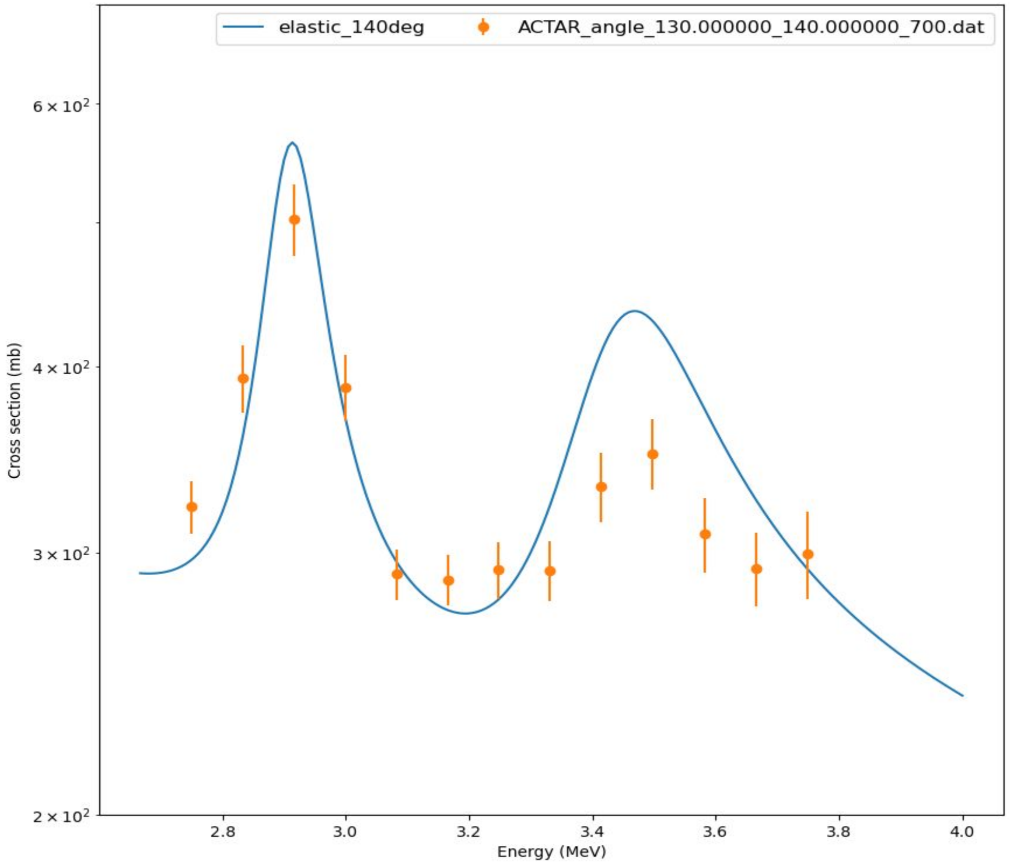


$^{4}He+^{8}He$ and $^{11}Be+n$ channels

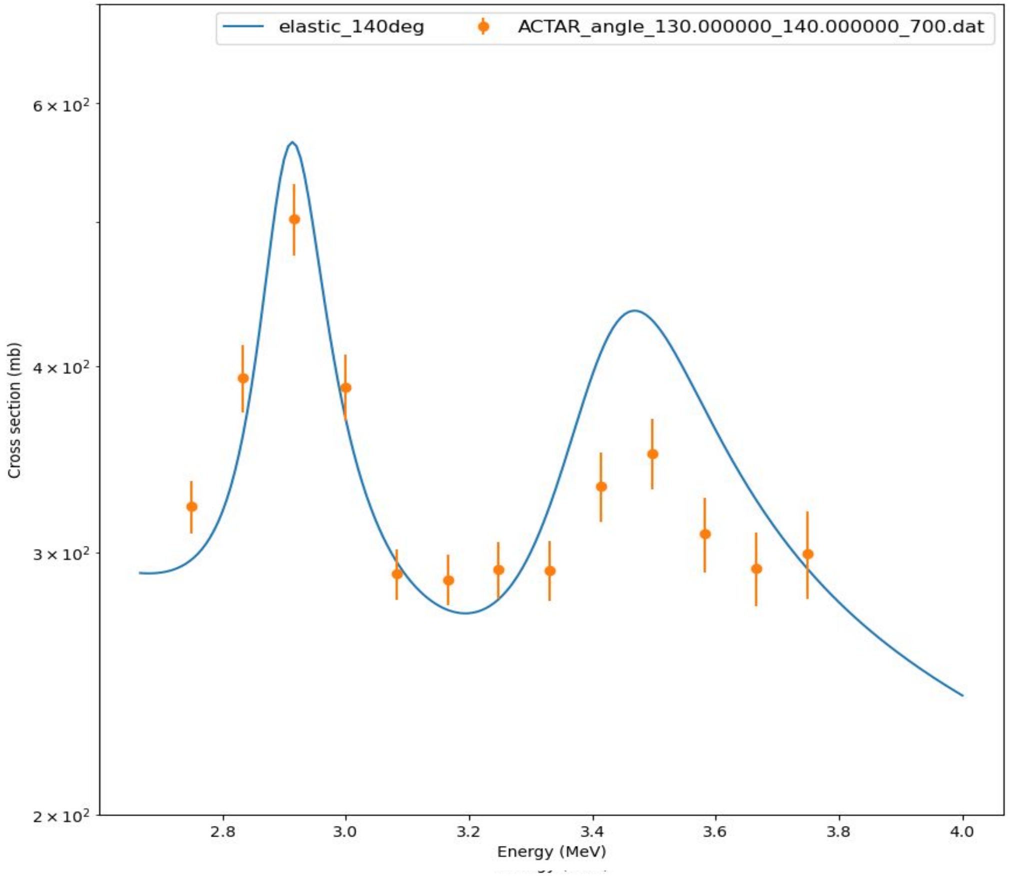

# R-Matrix fit

only $^{4}He$+$^{8}He$ channel

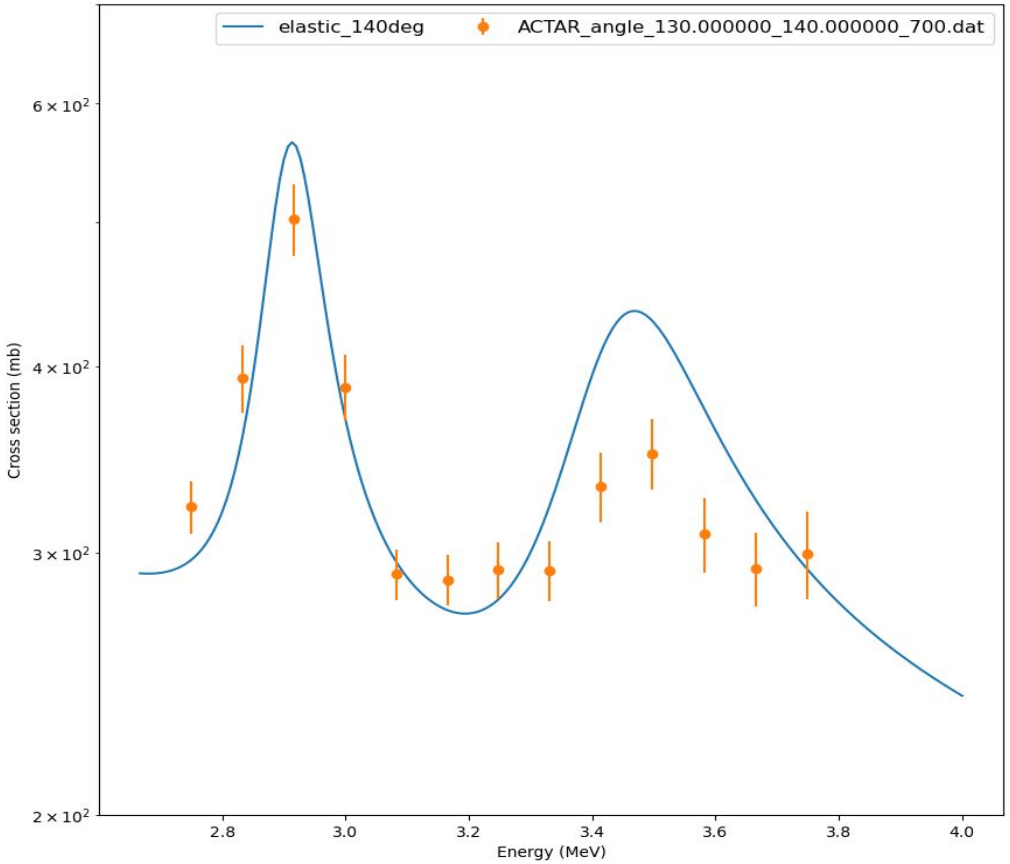


$^{4}He$+$^{8}He$ and $^{10}Be$+2n channels

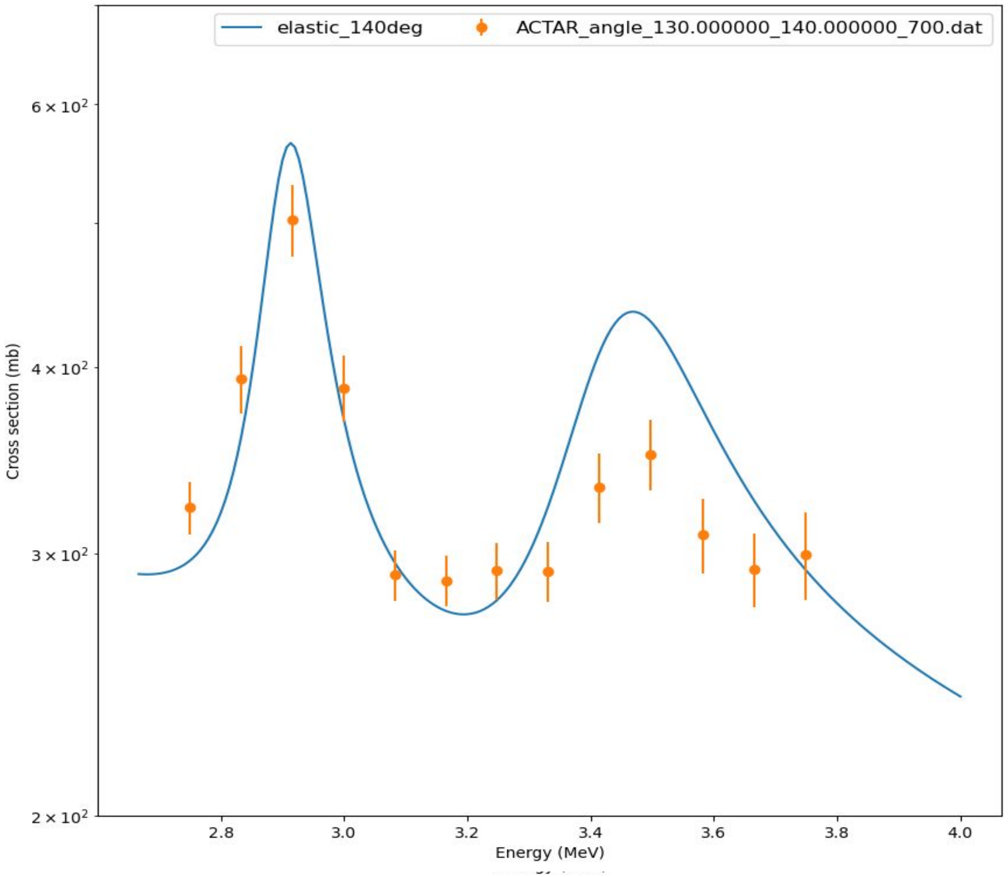

# R-Matrix fit

only $^{4}He+^{8}He$ channel

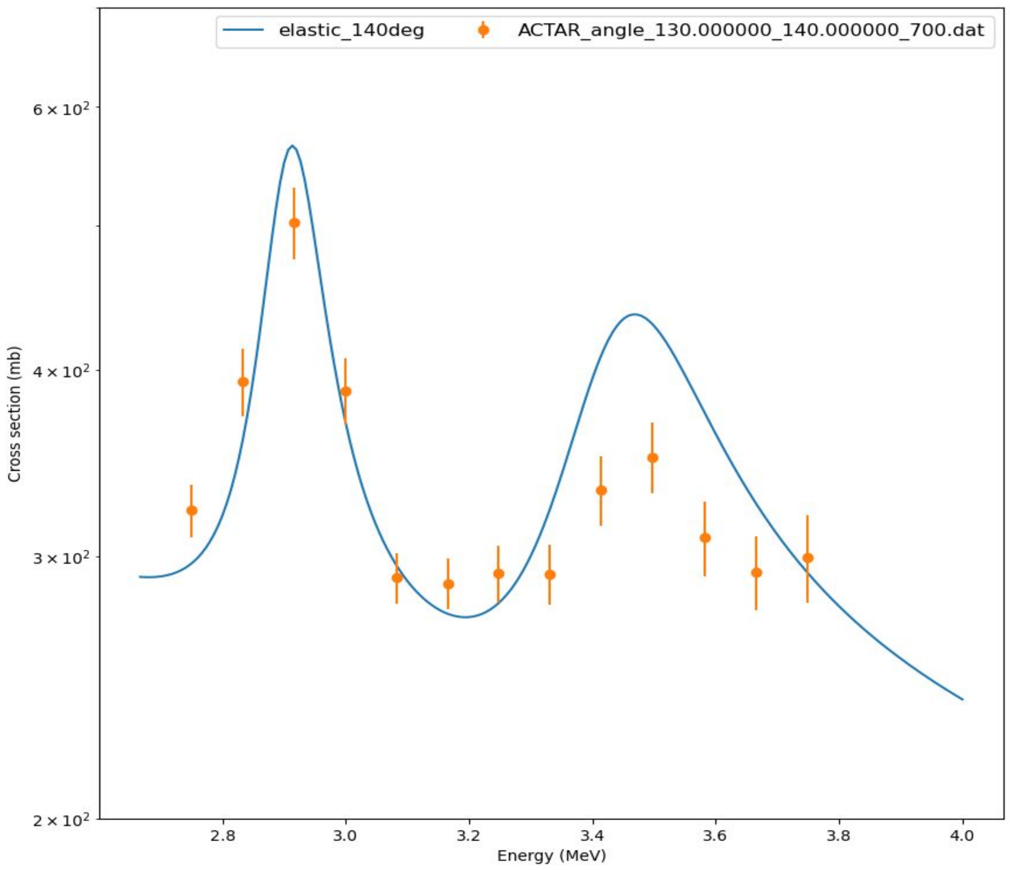


$^{4}He+^{8}He$ and $^{6}He+^{6}He$

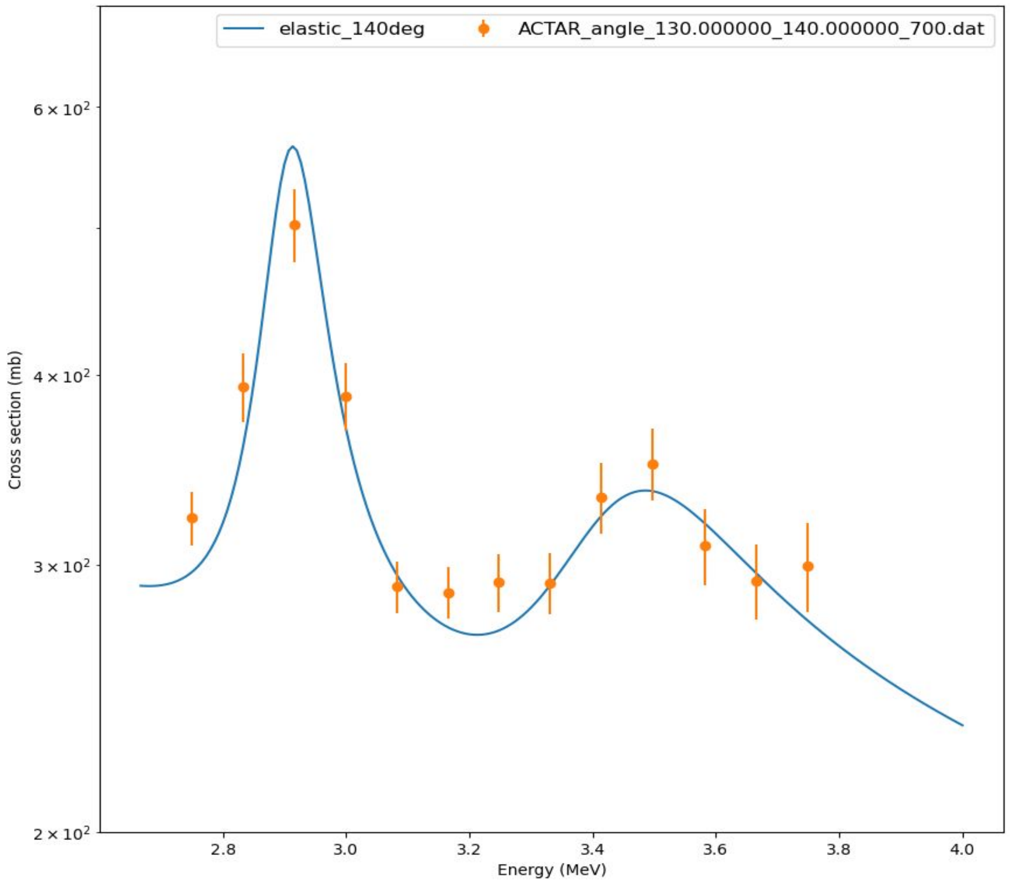

# Is the 5He+7He channel a problem for AZURE2?

- 5He and 7He are treated in the fit as effective two-body channel constituents (like stable particles), with a fixed threshold energy.
- In reality both are unbound resonances with large widths (5He: Γ = 648 keV; 7He: Γ = 160 keV) -> the "5He+7He threshold" is not a sharp energy but a broad region. This unbound nature is not explicitly built into the standard R-matrix treatment.
- Given the relatively small extracted width for this channel and its associated uncertainties, the approximation is not expected to significantly affect the present results.
- If a more precise description were required: an extended R-matrix formalism including sequential decay, or a dedicated few-body approach.

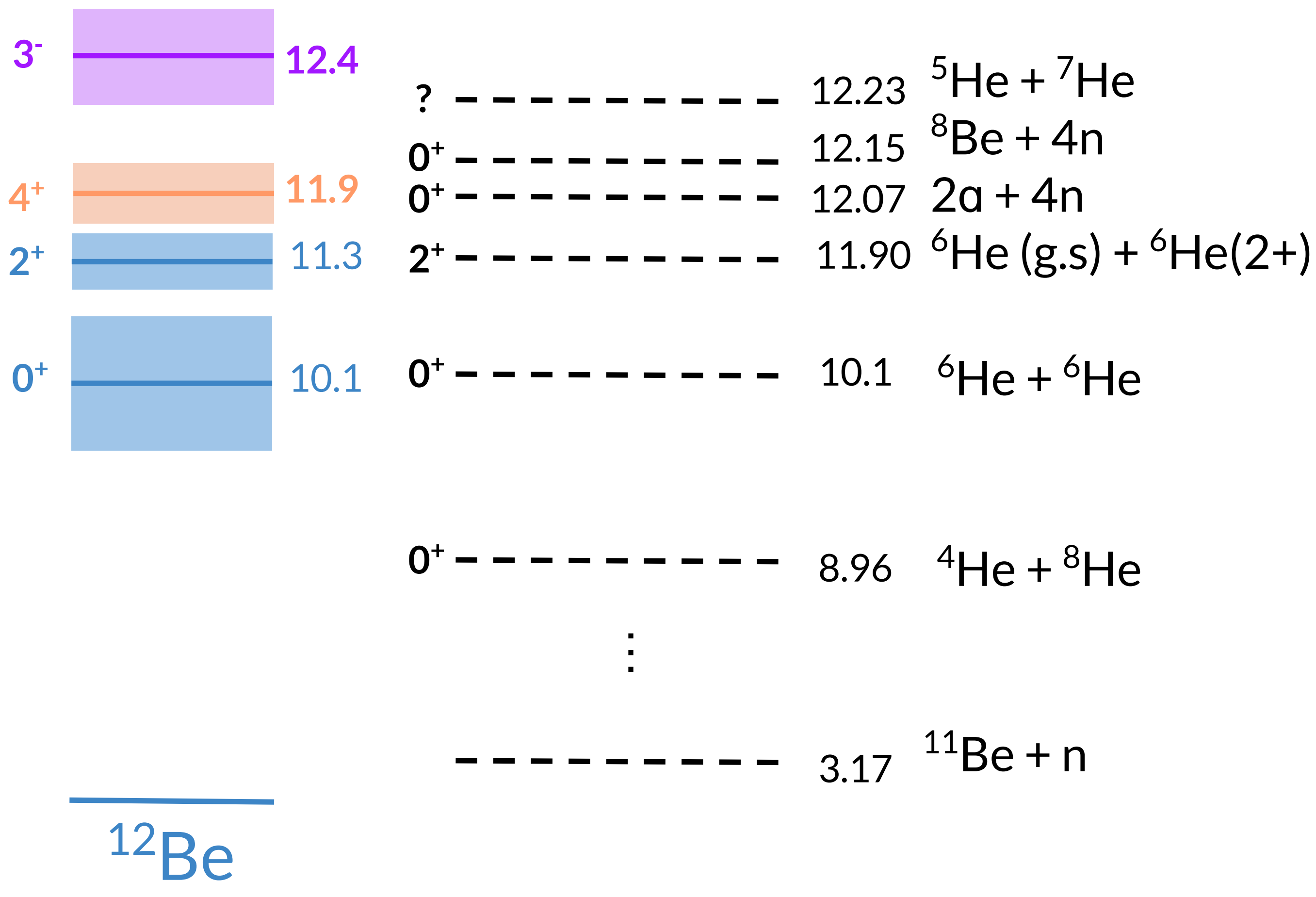

# No measured 6He

- 11.9 MeV - $4^+$ :

| channel | $\theta^2$ |
|---|---|
| $^4He+^8He$ | 0.86(12) |
| $^6He+^6He$ | 0.24(20) |
| $^{11}Be+n$ | 0.001(1) |

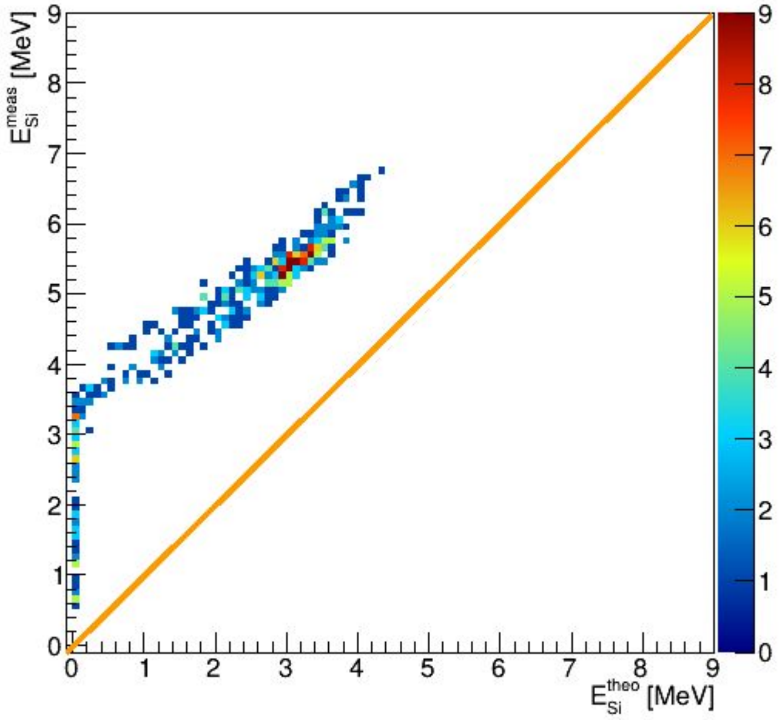


- dominant $^4He$ + $^8He$ structure
- minor $^6He+^6He$ mixing

No $^6He$ from the $^6He+^6He$ channel is observed in the data
Maximum undetected $\theta^2$ in ACTAR TPC: **0.28**

↩

# No measured 6He

As introduced in the previous section, we observe a state at $E_x = 11.9$ MeV in $^{12}$Be for the $^4$He($^8$He,$^8$He)$^4$He reaction, corresponding to approximately 100 counts. Assuming this state is the predicted $4^+$ state calculated at 11.99 MeV using the Generator Coordinate Method (GCM) [43], we can interpret the absence of $^6$He+$^6$He events in light of theoretical and experimental constraints.

According to the GCM calculations, the partial width ratio between the $^6$He+$^6$He and $^4$He+$^8$He decay channels is:

$$\frac{\Gamma_{^6He+^6He}}{\Gamma_{^4He+^8He}} \approx 0.07, \tag{II.30}$$

while our experimental measurement yields a ratio of $\approx 0.12$.
Combined with simulations that estimate a detection efficiency ratio of:

$$\frac{N_{^6He+^6He}}{N_{^4He+^8He}} \approx 0.47, \tag{II.31}$$

the expected number of $^6$He+$^6$He counts is:

$$N^{counts}_{^6He+^6He} \approx 100 \times 0.07 \times 0.47 \approx 3 \text{ counts (GCM ratio).} \tag{II.32}$$

Using our experimentally extracted ratio instead:

$$N^{counts}_{^6He+^6He} \approx 100 \times 0.12 \times 0.47 \approx 5 \text{ counts (experimental ratio).} \tag{II.33}$$

Such low count rates could easily fall below detection thresholds or be excluded by background subtraction, pile-up effects, or event selection criteria, which explains the absence of a clear $^6$He+$^6$He signal in the data.

# No measured 6He

- **12.4 MeV - $3^-$** :

| channel | $\theta^2$ |
|---|---|
| $^{4}He+^{8}He$ | 0.21(2) |
| $^{6}He+^{6}He$ | 0.02(3) |
| $^{11}Be+n$ | 0.01(1) |
| $^{5}He+^{7}He$ | 0.88(30) |
| $^{8}Be+4n$ | 0.49(40) |

No $^{6}He$ from the $^{6}He+^{6}He$ channel is observed in the data
Maximum undetected $\theta^2$ in ACTAR TPC: **0.04**

↩

# Comparison with literature

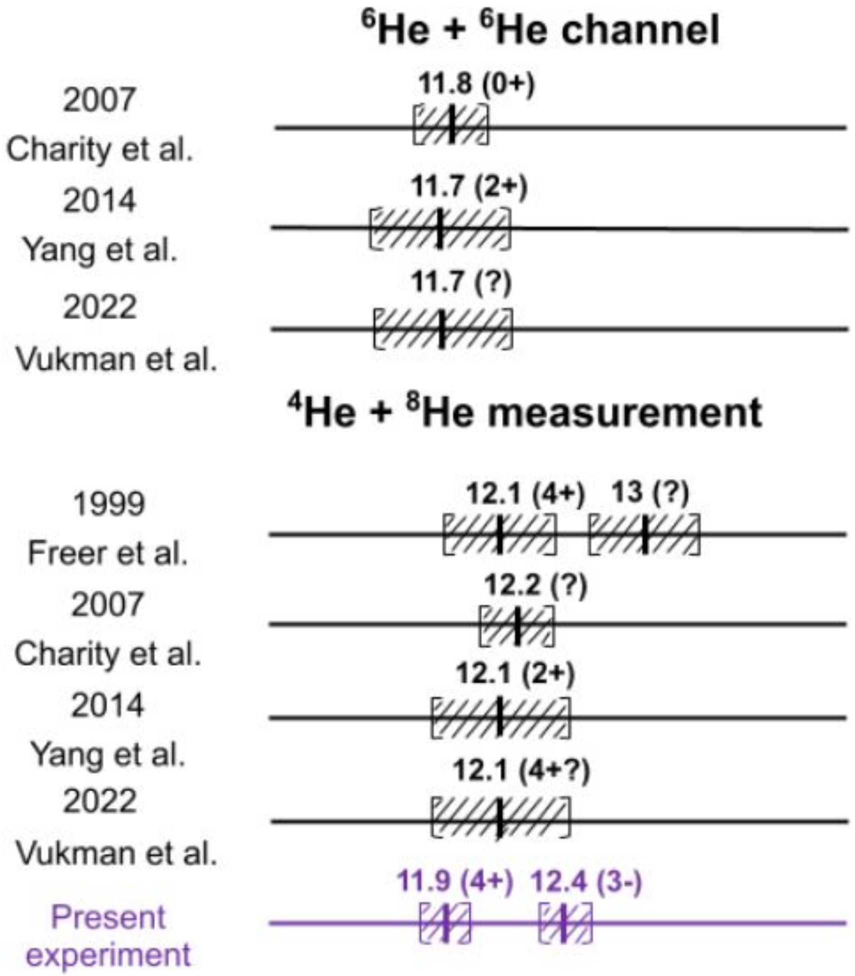


Figure II.72: Review of previously reported states of $^{12}Be$ in the literature, compared with the two resonances observed in the present work in the excitation energy range $E_x = 11.6$–$13$ MeV.

↩

# Comparison with theory

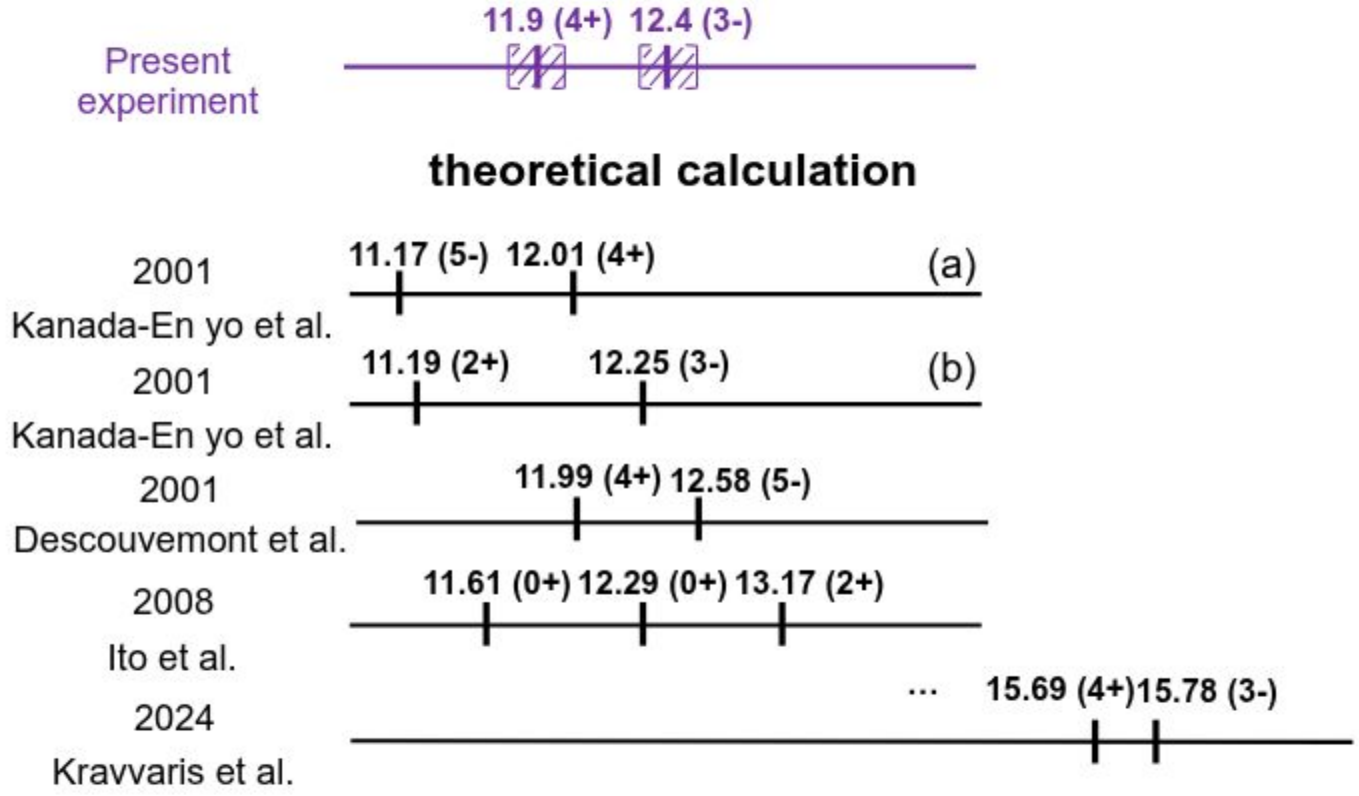


Figure II.74: Review of the predicted states of $^{12}Be$ compared to the two new levels observed in this work. See details on theoretical works in text.

# Rotational bands

- Collective excitations in **deformed nuclei**

$$E_J = E_0 + \frac{\hbar^2}{2I} J(J+1)$$

with I: moment of inertia → measure of **deformation**

- **Clustered** nuclei → deformed → rotational motion
- **Neutron-rich systems:**
  - **π orbitals:** compact/triaxial
  - **σ orbitals:** elongated/prolate

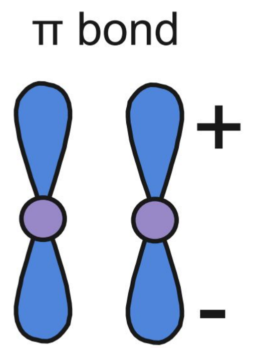


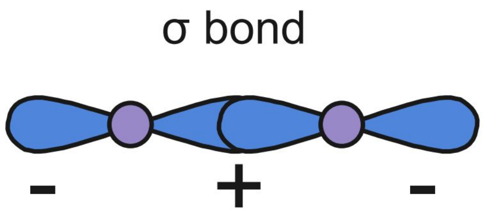


-> Rotational bands reveal **shape**, **deformation**, and **cluster structure** in nuclei

# Rotational band in $^{12}Be$

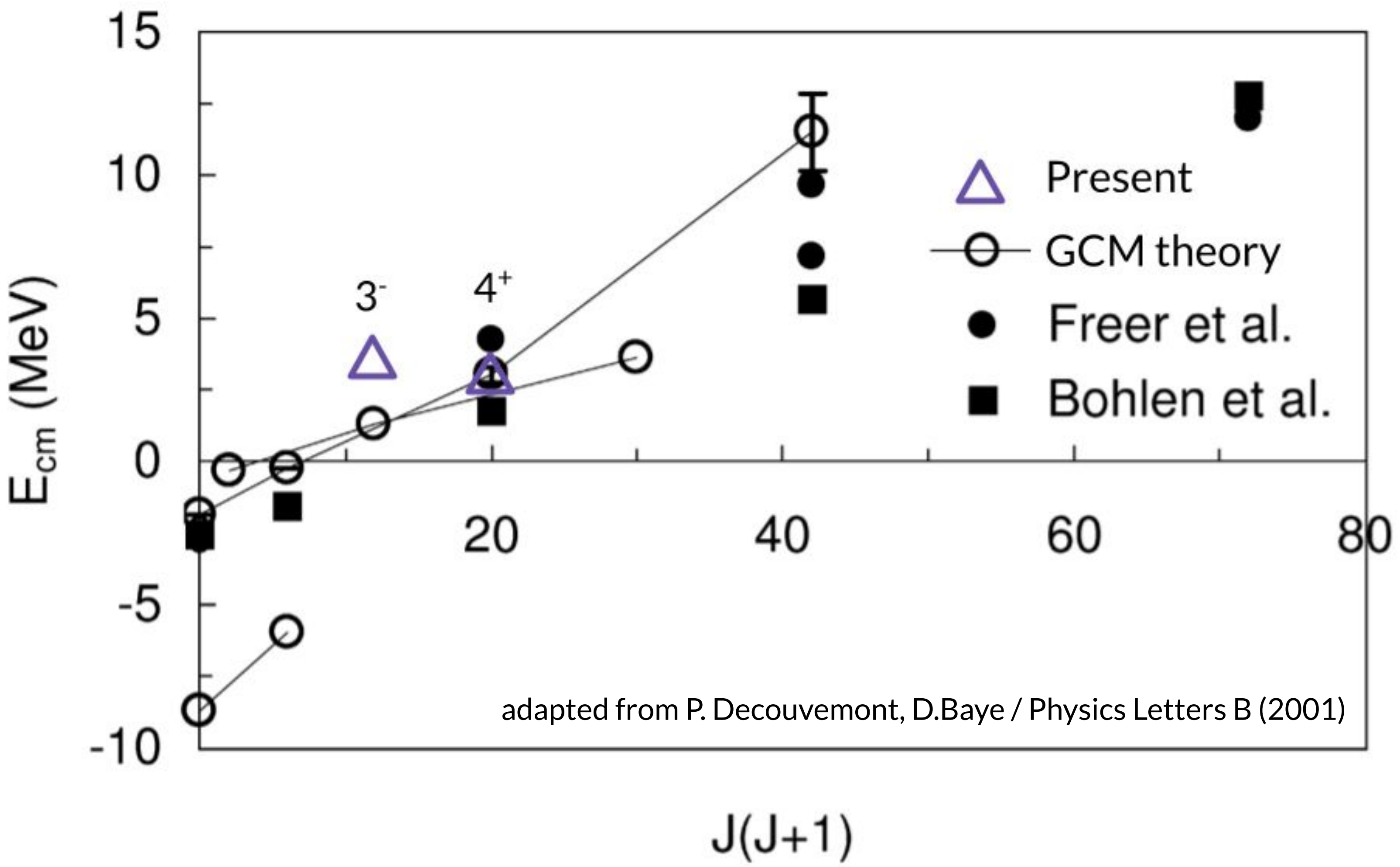

adapted from P. Decouvemont, D.Baye / Physics Letters B (2001)

-> 4+ part of the molecular band

↩

# Rotational band in Be isotopes

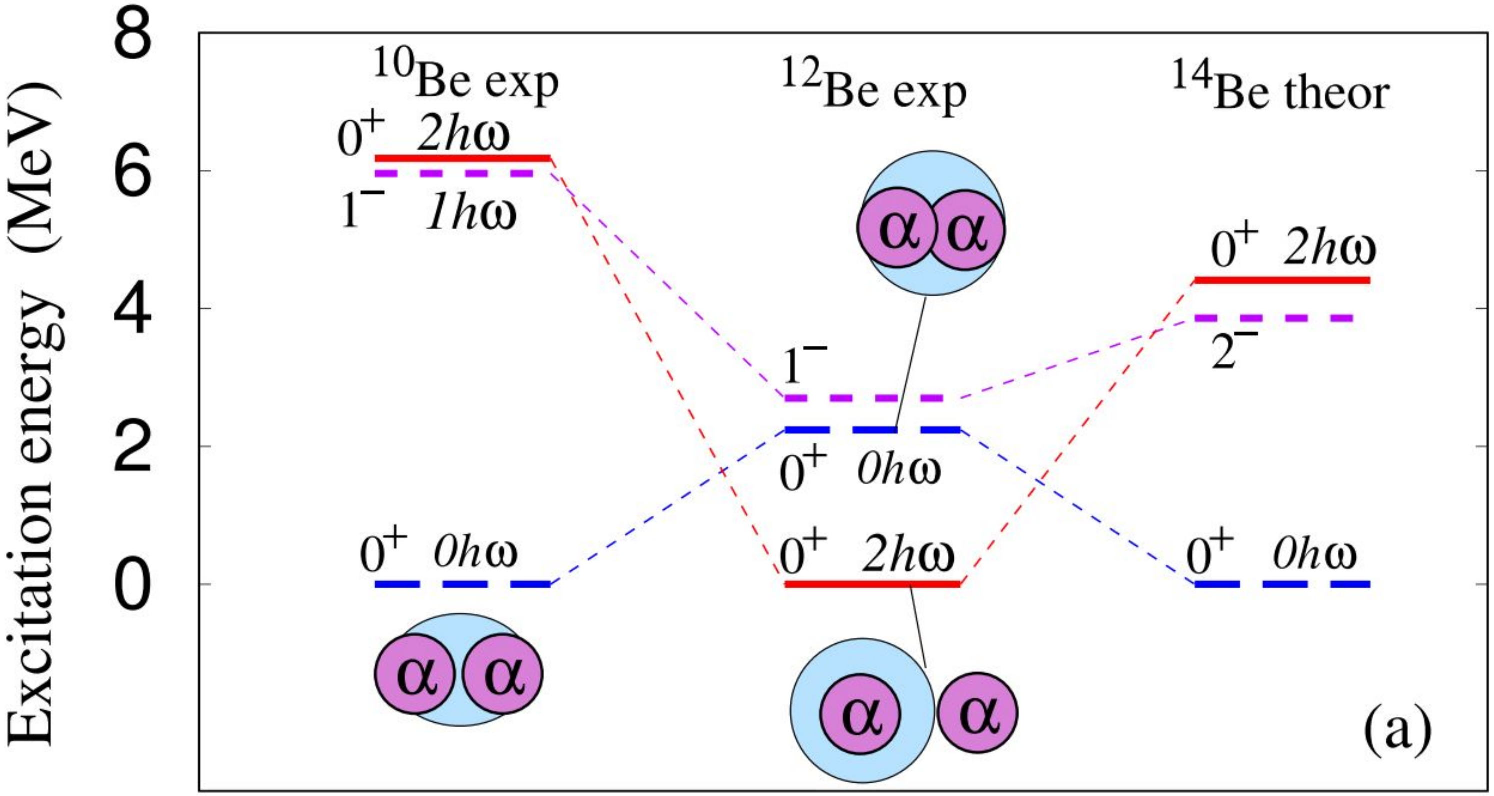


Tanigushi et al. (2025)

↩

# Rotational band in Be isotopes

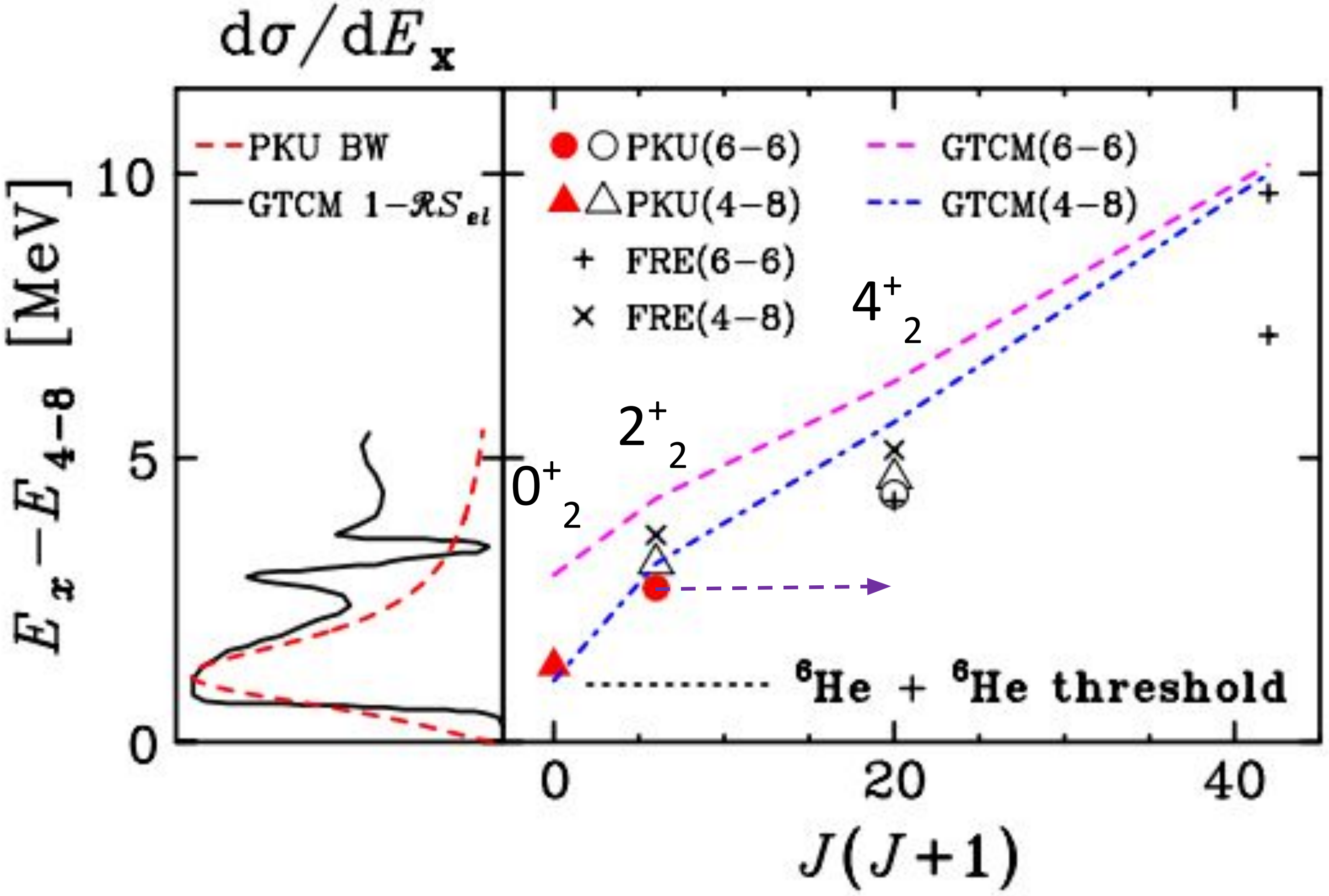


Yang et al. (2014)

↩

# Rotational bands in $^{12}Be$

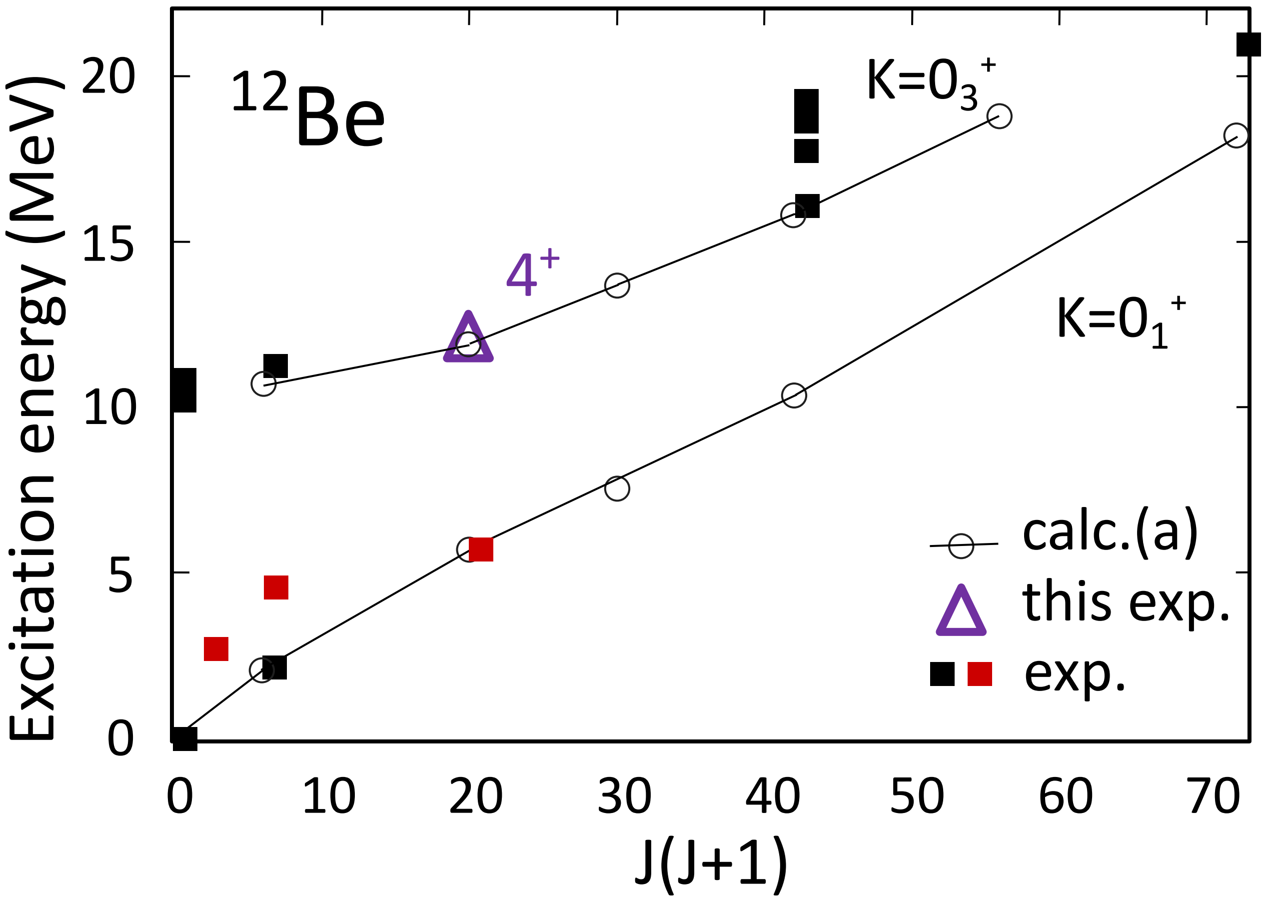


- **$^{12}$Be cluster structures:** $^{8}$He+$^{4}$He and $^{6}$He+$^{6}$He configurations.
- **Ground state ($0_1^+$):** Dominated by $^{8}$He+$^{4}$He clustering.
- **Highly excited states ($0_3^+$):** Band shows $^{6}$He+$^{6}$He cluster resonance.
- **N = 8 magic number breaking:** 0ħω–2ħω configuration inversion in $^{12}$Be.

(a) AMD+VAP Tanigushi et al. (2025)

↩

# Rotational bands in $^{12}Be$

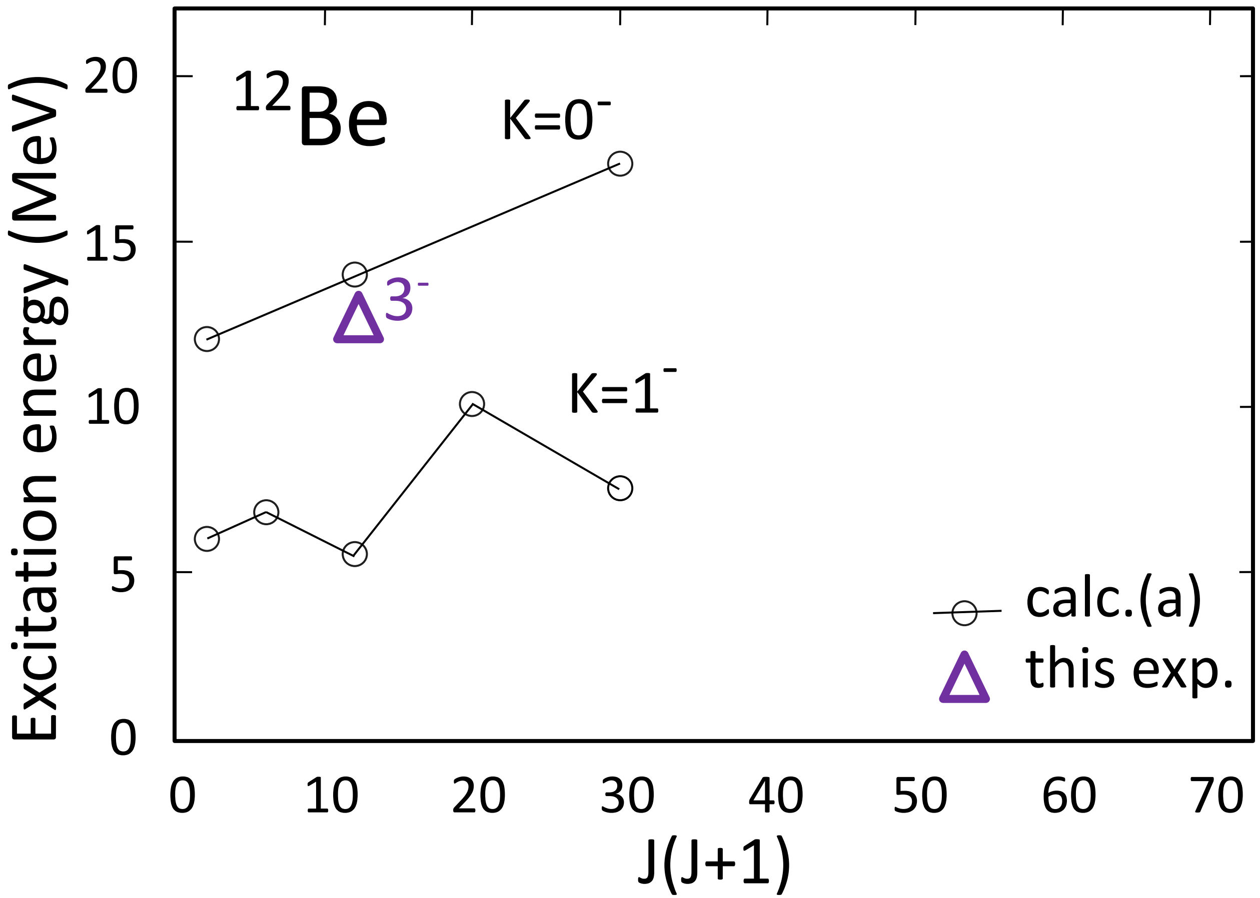


(a) AMD+VAP Tanigushi et al. (2025)

- **K=0⁻ band:** $^{8}He + ^{4}He$ cluster resonance, Parity partner of the ground band $K=0_1^+$
- **K=1⁻ band:** Molecular−orbital structure, valence neutrons occupy π and σ orbitals around the 2α core

↩

# Rotational band in Be isotopes

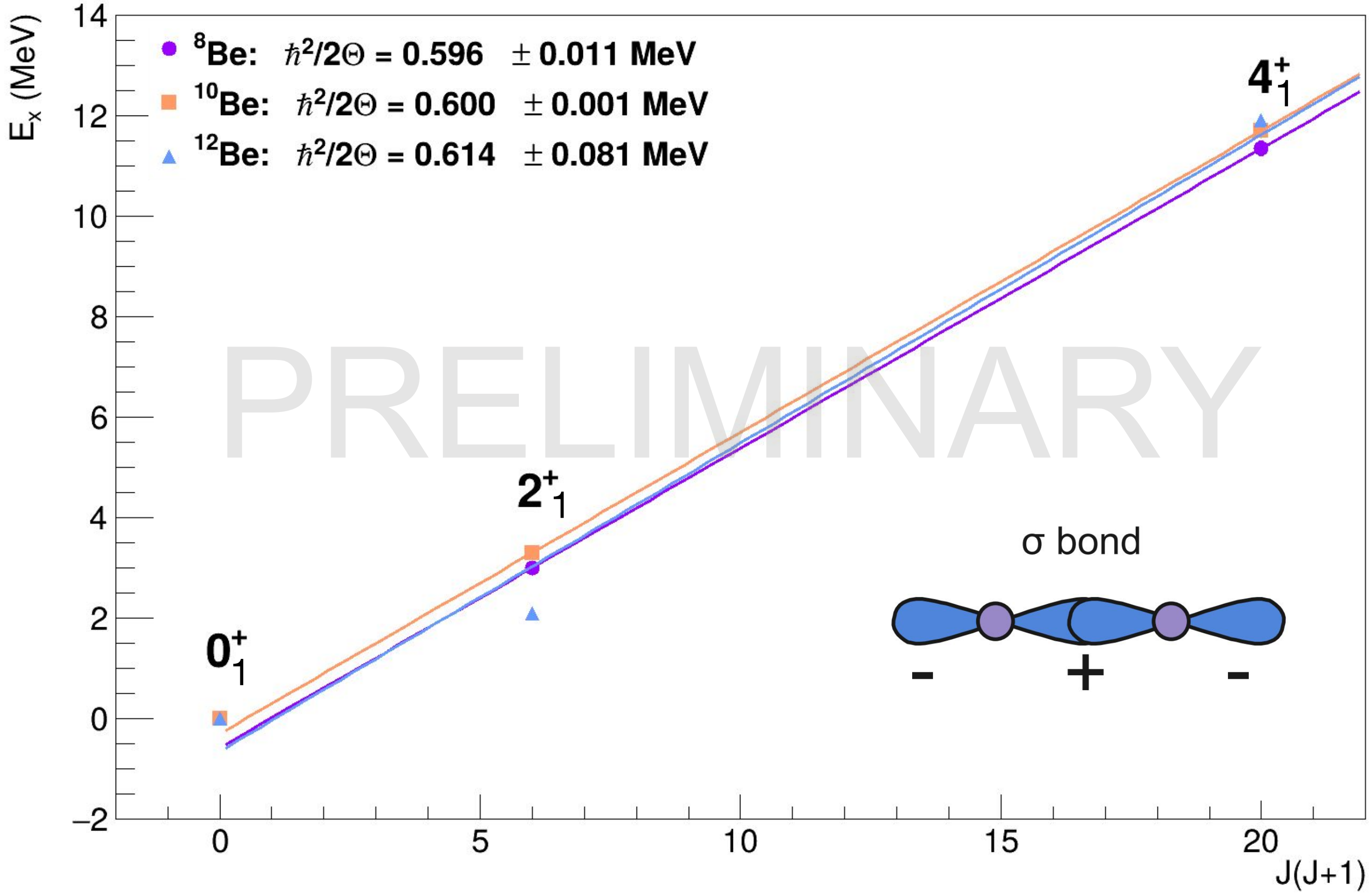


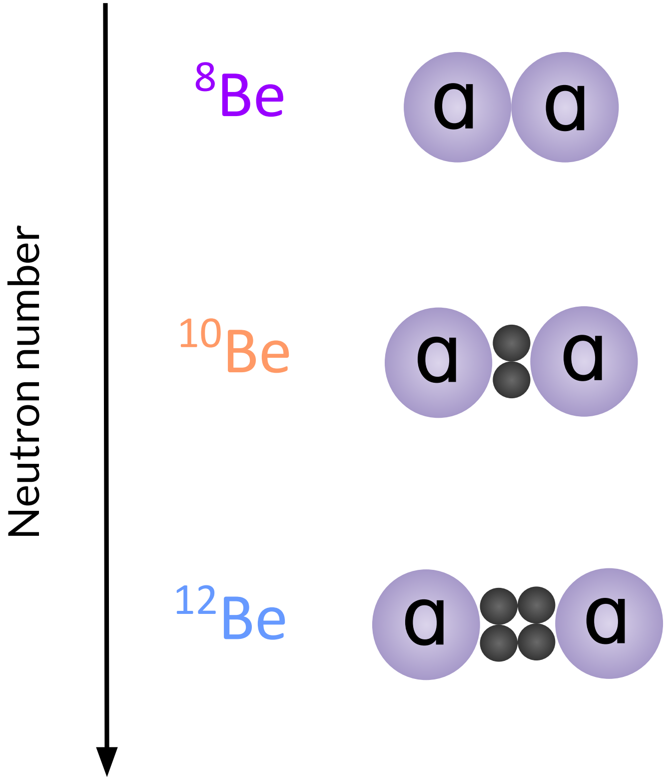


-> Confirms that **α-cluster cores coupled with valence neutrons** generate **collective rotational excitations** in **neutron-rich Be isotopes ($^{10}$Be, $^{12}$Be)**, extending the rotational behavior observed in the **pure α–α system of $^8$Be**.

# Rotational band in Be isotopes

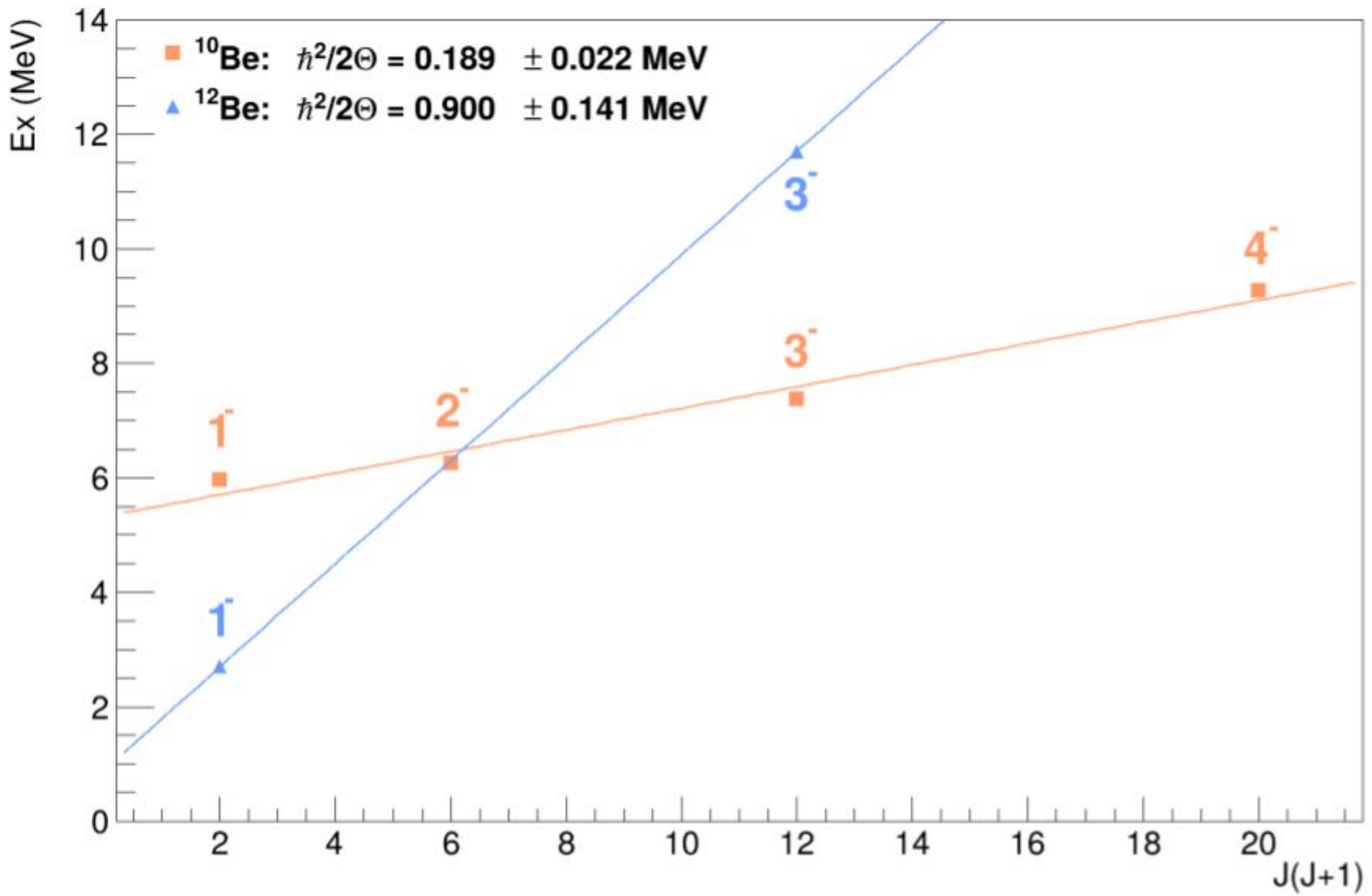


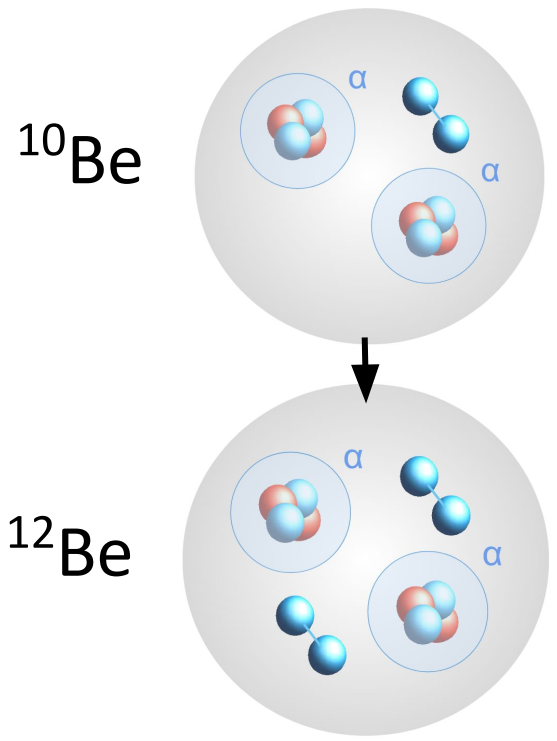


-> **Difference in rotational parameters** highlights the strong **influence of valence neutrons** on **nuclear deformation** and **rotational dynamics**.

↩

# Rotational band in Be isotopes